The Portugal Coastal Counter Current off NW Spain: New Insights on its Biogeochemical Variability

X.A Álvarez–Salgado[1,*], F.G. Figueiras[1], F.F. Pérez[1], S. Groom[2], E. Nogueira[1,3], A.V. Borges[4], L. Chou[5], C.G. Castro[1], G. Moncoiffé[6,7], A.F. Ríos[1], A.E.J. Miller[8], M. Frankignoulle[4], G. Savidge[6], R. Wollast[5]

[1]CSIC, Instituto de Investigacións Mariñas, Eduardo Cabello 6, 36208–Vigo, Spain

[2]CCMS, Plymouth Marine Laboratory, Prospect Place, Plymouth PL1 3DH, UK.

[3]IEO, Centro Oceanográfico de Gijón, Avda. Príncipe de Asturias 70 bis, 33212–Gijón, Spain

[4]University of Liège, Unité d'Océanographie Chimique, Sart Tilman B5, B–4000 Liège, Belgium

[5]Laboratoire d'Océanographie Chimique et Géochimie des Eaux, Université Libre de Bruxelles, Campus de la Plaine – CP 208, B–1050 Brussels, Belgium

[6]Queen's University of Belfast, Dept. of Environmental Sciences, Marine Laboratory, Portaferry, BT22 1PF C. Down, North Ireland, UK.

[7]BODC, Bidston Observatory, Bidston Hill, Prenton CH43 7RA, UK.

[8]SAMS, Univ. of the Highlands & Islands project, Dunstaffnage Marine Laboratory, Oban, Argyll PA34 4AD, UK

* Corresponding author: xsalgado@iim.csic.es, phone: +34 986 231930, fax +34,986 292762

Version : 27 June 2002

Abstract

Available time–series of wind–stress data, AVHRR and SeaWiFS satellite images, and *in situ* data from seven cruises are used to assemble a coherent picture of the hydrographic variability of the NW Iberian Peninsula from the onset (September–October) to the cessation ((February–May) of the Portugal Coastal Counter Current (**PCCC**), a clearly under sampled period from the view point of the chemistry and the biology of shelf, slope and ocean waters in the 40º–43ºN latitudinal range. Novel information extracted from these observations refers to: **1**) the most frequent modes of variability of alongshore coastal winds, covering event, seasonal and long–term scales; **2**) the conspicuous stratification/homogenisation cycle observed in **PCCC** waters, with key implications for the chemistry and biology of this hydrographic structure; **3**) the seasonal evolution of nitrite profiles in **PCCC** waters in relation to the stratification/homogenisation cycle; **4**) the Redfieldian stoichimetry of the mineralization of organic matter in oceanic Eastern North Atlantic Central Water (ENACW) transported by the **PCCC**: **5**) The separation of coastal (mesotrophic conditions) and **PCCC** (oligotrophic conditions) plankton populations by a downwelling front on the shelf, which displaces across shore as a function of coastal wind intensity and continental runoff; and **6**) the photosynthetic response of PCCC and coastal plankton populations to the changing stratification and light conditions from the onset to the cessation of the **PCCC**.

Keywords: seasonal cycle, upwelling, downwelling, hydrography, biogeochemistry, Portugal Current System

Glossary of terms

α^B	Photosynthetic efficiency of P–E relationships ($\frac{gC(gChl)^{-1}h^{-1}}{\mu molm^{-2}s^{-1}}$)
AOU	Apparent oxygen utilisation (μmol kg^{-1})
AVHRR	Advanced very high resolution radiometer
C_T	Total inorganic carbon (μmol kg^{-1})
CTZ	Coastal transition zone
DCM	Deep chlorophyll maximum
E_k	Light saturation parameter of P–E relationships (μmol m^{-2} s^{-1})
ENACW	Eastern North Atlantic Central Water
ENACWsp	ENACW of subpolar origin
ENACWst	ENACW of subtropical origin
NAO	'North Atlantic Oscillation' index
NC_T	C_T normalised to salinity 35.0 (μmol kg^{-1})
NTA	TA normalised to salinity 35.0 (μmol kg^{-1})
PAR	Photosynthesis available radiation
PNM	Primary nitrite maximum
P_m^B	Maximum photosynthetic rate of P–E relationships (g C (g Chl)$^{-1}$ h^{-1})
PCCC	Portugal coastal counter current
P–E	Photosynthesis–irradiance relationships
PP	Primary production (mg C m^{-2} d^{-1})
$-Q_X$	Offshore Ekman transport (m^3 s^{-1} km^{-1})
R	Continental runoff (m^3 s^{-1})
S[*NAO*]	Cumulative sum function of the NAO index
S[$-Q_X$(t)]	Cumulative sum function of $-Q_X$
SC[$-Q_X$]	Seasonal cycle of $-Q_X$
SeaWiFS	Sea–viewing Wide Field–of–view Sensor
SSS	Sea surface salinity
SST	Sea Surface Temperature (ºC)
TA	Total Alkalinity (μmol kg^{-1})

Contents

1. Introduction

A poleward–flowing slope undercurrent centred at 150–300m depth, compensating the equatorward–flowing surface circulation, is a common feature of the coastal upwelling systems of California/Oregon, Peru/Chile, Namibia/Benguela and Canary/Iberian Peninsula (Smith, 1989). There is evidence of poleward undercurrents from tropical to polar latitudes along the eastern boundaries of all the main oceans (Pingree, 1994), these primarily being forced by large–scale geopotential gradients and topography (McCreary, Shetye, & Kundu, 1986; Frouin, Fiúza, Ambar & Boyd, 1990; Huthnance, 1995). Surface countercurrents are also common in major coastal upwelling systems, either as surface manifestations of trapped waves or surfaced undercurrents (Mooers, 1989). Surfacing of undercurrent waters occurs at latitudes affected by a marked seasonal reversal in wind stress and curl. Examples of this surfacing are found in the Hiada Current off Western Canada (Freeland, 1989), the Davidson Current in the California Current System (Huyer, Kosro, Lentz, & Beardsley, 1989), and the Portugal Coastal Counter Current (**PCCC**) in the Portugal Current System (Ambar & Fiúza, 1994). All these surface countercurrents manifest during autumn and winter, when local winds blow from the S–SW, forcing poleward displacement of the surface wind–mixed layer and a convergence front with coastal waters. An extreme case of surface countercurrent is found in the Leeuwin Current, off Western Australia (Cresswell & Golding, 1980; Smith et al., 1991). The largest along–shore geopotential gradient ever observed in any eastern boundary region prevents the development of a steady equatorward flow, despite favourable wind–stress during the spring and summer (Church, Cresswell & Godfrey, 1989; McCreary et al., 1986).

The dynamics (fronts, centres and filaments) and biogeochemistry (primary production, recycling and shelf–ocean exchange) of coastal upwelling systems have been the subject of recent research conducted off California (Brink & Cowles, 1991), NW Africa (Barton et al., 1998) and NW Iberia (Joint, Inall Torres–Almarza, Figueiras, Álvarez–Salgado & Woodward, 2001) carried out under the auspices of ambitious ‘Coastal Transition Zone’ programmes. Much less attention has been paid to the surface countercurrents that develop during prolonged downwelling–favourable periods: up to 6 months per year in temperate latitudes (Wooster,

Bakun & McLain, 1976; Huyer et al., 1989). The surface countercurrent regime **1**) conducts salt, heat, dissolved substances and plankton assemblages from subtropical to temperate/subpolar latitudes along the slope and **2**) prevents, or even reverse, the off–shelf export of materials characteristic of coastal upwelling systems (Pingree, Sinha & Griffiths, 1999).

Ambar and Fiúza (1994) have reviewed the surface circulation off the Western Iberian Peninsula. The area is dominated by the Portugal Current System, which is composed of **1**) the Iberian basin scale, slow, equatorward circulation of the Portugal Current proper in the open ocean (Richardson, 1983; Krauss & Kase, 1984; Arhan, Colin de Verdière & Memery, 1994); and **2**) the Iberian slope scale, fast, seasonally reversing Portugal Coastal Current near the coast. During the summer, the 30–40 km wide and 50–100m deep Portugal Coastal Current flows southward in the vicinity of the shelf break, driven by upwelling–favourable northerly winds. The flow transports cold and nutrient–rich recently upwelled Eastern North Atlantic Central Water of subpolar origin (>45°N; ENACWsp) in the north and warmer and nutrient–poorer ENACW of subtropical origin (<40°N, ENACWst) in the south (Fiúza, 1984; Ríos, Pérez & Fraga, 1992; Pérez, Mouriño, Fraga & Ríos, 1993). During September–October the surface circulation reverses to constitute the well–defined 30 km wide and 200m deep **PCCC** off the NW Iberian Peninsula, which is the subject of the present study. The **PCCC** is present until March–April (Wooster et al., 1976; Ambar, Fiúza, Boyd & Frouin, 1986; Frouin et al., 1990), transporting ENACWst from at least 39°N (off Lisbon) —where it appears to be considerably wider— to 47°N (the Armorican Shelf off SW France; Pingree & Le Cann, 1990). Following Pingree et al. (1999), the coastal current system off NW Spain is a component of the predominantly density and topographically driven European 'Poleward Slope Current'.

The dynamics of the **PCCC** has been studied using AVHRR satellite images (Ambar et al., 1986; Pingree & Le Cann, 1990; Frouin et al., 1990), *in situ* hydrographic data accompanied by geostrophic calculations (Haynes & Barton, 1991; Mazé, Arhan & Mercier, 1997; Fiúza, Hamann, Ambar, Diaz del Río, González & Cabanas, 1998), current meter records (Swallow, Gould & Saunders, 1977; Ambar et al., 1986), and surface drifters (Haynes & Barton, 1990).

However, little attention has been paid to the biogeochemical implications of poleward surface flows either in the Portugal Current System or in the eastern boundary current systems in other oceans. Indeed, it appears that the studies by Bode, Fernández, Botas and Anadón (1990) off N Spain in April 1987 and Castro, Álvarez–Salgado, Figueiras, Pérez and Fraga (1997) off NW Spain in September 1986 are unique in focusing on the biogeochemistry of these systems. Both studies found isolated communities of organisms associated with particular chemical (low NO_3^-, high NO_2^-) and physical conditions. More recently, Peliz and Fiúza (1999) analysed Coastal Zone Colour Scanner (CZCS) images and showed a wedge of southern oligotrophic water penetrating northward over the western Iberian continental margin during the autumn and winter, between the pigment–rich shelf zone and the moderate concentrations offshore.

Data from some of the seven research cruises employed in this work has been previously used to describe the thermohaline (Ríos et al., 1992; Pérez, Ríos, King, & Pollard, 1995; Fiuza et al., 1998) and chemical (Pérez et al., 1993; Pérez, Castro, Álvarez–Salgado, & Ríos, 2001) characteristics of ENACW in ocean waters off NW Spain, the rapid ageing of ENACW on the shelf (Álvarez–Salgado, Castro, Pérez, & Fraga, 1997; Prego & Bao, 1997), the behavior of surface waters as a source–sink for atmospheric CO_2 (Pérez, Ríos, & Rosón, 1998; Borges, & Frankignoulle, 2002), and the satellite–derived primary production in NW Iberian shelf, slope and open ocean waters (Joint, Groom, Wollast, Chou, Tilstone, Figueiras, Loijens & Smyth, 2002). Consequently, this work will be essentially focused on those issues that have not been studied yet, such us **1**) an statistical approach to the recurrent modes of variability of coastal winds, covering from long–term to daily time–scales (section 3.1), **2**) the seasonal cycle of stratification–homogenisation of **PCCC** waters, with key implications for the chemistry and biology of the area (section 3.2.3), **3**) the O_2/C/N/P/Si stochiometry of organic matter mineralisation in oceanic ENACW transported by the **PCCC** (section 3.3.1), **4**) the seasonal development of nitrite profiles in **PCCC** waters in relation to the stratification–homogenisation conditions (section 3.3.2), **5**) the plankton species composition in NW Iberian waters during the PCCC–favourable season (section 3.4.2) and **6**) the photosynthetic response of these species under contrasting stratification–homogenisation conditions (section 3.4.3). We will base our

analyses on wind–stress and offshore Ekman transport calculations, AVHRR and SeaWiFS satellite images and a set of hydrographic cruises covering the onset of the **PCCC** (September–October), through the period of maximum winter convection to the cessation of the **PCCC** (April–May). The study will be restricted to the 40°–43°N latitudinal range.

2. Materials and methods

2.1. The set of hydrographic cruises

Mapping of relevant thermohaline, chemical and biological variables was performed during the course of seven hydrographic cruises conducted off the NW Iberian Peninsula between 1983 and 1998 (**Fig. 1**). Cruise GALICIA–XII (10 to 18 September 1991) coincided with the onset of the **PCCC** in the period of maximum stratification during the transition from upwelling– to downwelling–favourable winds. Cruises GALICIA–VI (1 to 12 December 1983) and MORENA–II (15 November to 2 December 1993) show an advanced state of development of the **PCCC** in late autumn. The former cruise covers from 42° to 44°N (off NW Spain), whereas the latter extends from 40° to 42°N off Northern Portugal. Cruises CD110b (6 to 16 January, 1998) and GALICIA–VII (18 February to 7 March 1983) were carried out during the winter mixing period. Finally, cruise MORENA–I (10 to 26 May 1993) was conducted just before the onset of the upwelling season in the survey area. Data from cruise Bg9815c (26 June to 7 July 1998) will be used to illustrate the situation when the Portugal Coastal Current flows southwards in the direction of the dominant upwelling favourable northerly winds and the poleward flow is observed as a subsurface slope undercurrent.

Cruises GALICIA–VI (December 1983) and GALICIA–VII (February–March 1984) were performed during the same downwelling season (1983–84), allowing comparison of the hydrographic changes occurring in the **PCCC** before and after a winter mixing period without any influence of inter–annual variability. Notable poleward surface flow occurred during the winter 1983–84 with conspicuous warming along the north Spanish coast around New Year (Pingree & Le Cann, 1989). Similarly, cruises MORENA–I (May 1993) and MORENA–II (November–December 1993) were conducted before and after the upwelling–favourable season

in 1993, allowing comparison of the spring and autumn **PCCC** within the same year. Although only four stations were occupied during CD110b (January 1998) due to inclement weather conditions, data from the cruise has been included because it provides a unique view of conditions observed during January.

Table 1 summarises core information about the set of cruises, including research platform, study period, sampling devices, and measured variables. **Figure 1** indicates the location of sampling sites where vertical profiles of the different variables were obtained during each cruise. Plankton counts were not conducted during the 1983–1984 cruises and primary production data are only available for cruises MORENA–I, GALICIA–XII, CD110b and Bg9815c.

Nutrient concentrations were determined by the 'Instituto de Investigacións Mariñas–Group of Oceanography' using standard segmented flow analysis techniques (Hansen & Grashoff, 1983; Mouriño & Fraga, 1985; Álvarez–Salgado, Fraga & Pérez, 1992). Potentiometric pH was measured in the NBS (National Bureau of Standards) scale with the classical 7.413 phosphate buffer in most cruises, following the procedure of Pérez and Fraga (1987a). During cruises CD110b and Bg9815c the electrode was calibrated in the Total Hydrogen Ion Concentration Scale with the TRIS and AMP buffers according to Dickson (1993). Total Alkalinity (TA) was measured by potentiometric end–point titration according to Pérez and Fraga (1987b), except for cruises CD110b and Bg9815c when classical Gran electro–tritration was used. Total inorganic carbon (C_T) was calculated from pH and TA using the carbon system equations. C_T and TA have been normalised to salinity 35.0 to produce the corresponding NC_T and NTA parameters, which depend only on the biological and geochemical activity in the study water parcel. Finally, dissolved oxygen was measured by the Winkler method using a potentiometric end–point determination. Apparent oxygen utilization, AOU= O_2sat–O_2, is calculated using Benson and Krause's equation (UNESCO, 1986) for oxygen saturation (O_2sat). Chlorophyll *a* (Chl–*a*) was estimated fluorometrically by the method of Yentsch & Menzel (1963).

2.2. Wind–stress and offshore–onshore Ekman transport calculations

The north (south) component of shelf wind–stress (τ_y) causes upwelling (downwelling) favourable offshore (onshore) Ekman transport values ($-Q_X$) along the NW Iberian margin (Wooster et al., 1976), which can be roughly estimated following Bakun's (1973) method:

$$-Q_X = \frac{\tau_y}{\rho_{SW} \cdot f} = -\frac{\rho_{air} \cdot C_D \cdot |V| \cdot V_y}{\rho_{SW} \cdot f} \quad (1)$$

where ρ_{air} is the density of air (1.22 kg·m^{-3} at 15°C), C_D is an empirical dimensionless drag coefficient (1.4·10^{-3} according to Hidy 1972), f is the Coriolis parameter (9.946·10^{-5} s^{-1} at 43° latitude), ρ_{SW} is the density of seawater (~1025 kg·m^{-3}) and $|V|$ and V_y are the average daily module and north component of the geostrophic winds in a 2º×2º cell centred at 43°N 11°W (**Fig. 1c**) assumed representative for the study area. Average daily geostrophic winds were estimated from atmospheric surface pressure charts, provided at 6 hours intervals by the 'Instituto Nacional de Meteorología'. Positive values of $-Q_X$ (m^3 s^{-1} km^{-1}) indicate upwelling–favourable offshore Ekman transport. Conversely, negative values of $-Q_X$ indicate downwelling–favourable onshore Ekman transport (see Lavín, Díaz del Río, Cabanas & Casas (1991) for further details).

The time series of daily values of $-Q_X$ from August 1981 to July 1998 (n = 6205) has been analysed (**Fig. 2a**). Values outside the lower extreme bound (LEB = $Q_1 - 3 \cdot H$ = –3200 m^3 s^{-1} km^{-1}) and upper extreme bound (UEB = $Q_3 + 3 \cdot H$ = 3022 m^3 s^{-1} km^{-1}) were rejected before time series analysis (Q_1 and Q_3 are the lower and upper quartiles and H is the inter–quartile range). The rejected values represented ~3% of the whole time series. Spectral and harmonic analysis (Poularikas & Seely, 1991), and differencing techniques (Ibanez, Dauvin & Ettienne, 1993) were applied to characterise the modes of temporal variability of $-Q_X$ from short–term to inter–annual scales.

2.3. Geostrophic flow calculations

Following Frouin et al. (1990), the geopotential anomaly at 10 dbar was computed relative to 350 dbar. Although water displacements at this reference level are significant (Mazé et al.,

1997), they are small when compared with the enhanced surface circulation in the area either during the upwelling– or the downwelling–favourable seasons. Therefore, our geostrophic computations strictly provide only a qualitative rather than a quantitative description of the geostrophic circulation patterns off NW Spain. A more appropriate reference level would be 2500db (Mazé et al., 1997). However, on certain of the cruises it was not possible to sample to this depth (GALICIA–XII, MORENA–II and Bg9815c). Comparison of the geopotential anomalies at 10 dbar referred to 350 and 2500 dbar for the MORENA–I cruise were reasonably correlated (r= +0.79, p< 0.05). For shelf stations, where the water depth (Z) is shallower than the reference level, the extrapolation method of Reid and Mantyla (1976) was used, which consist of extrapolating the horizontal gradients of the geopotential anomaly computed from the pairs of stations in deeper waters towards the stations with Z< 350 dbar.

2.4. Advanced Very High Resolution Radiometer (AVHRR) and SeaWIFS images

2.4.1 Sea–surface temperature

Sea–surface temperature was measured using the Advanced Very High Resolution Radiometer (AVHRR) series of instruments, flown on the US NOAA series of polar–orbiting satellites. Individual 1–km resolution, raw satellite passes were supplied by the NERC Satellite Receiving Station, Dundee, Scotland and processed following Miller, Groom, McManus, Selley & Mironnet (1997). Briefly, the thermal infra–red channels are calibrated (Planet, 1988) and SST is computed using the split window technique (McClain, Pichel, & Walton, 1985) with appropriate NOAA algorithms for a given AVHRR instrument. Clouds are detected and masked using a series of tests on the visible and infra–red channels (Miller et al., 1997) and images are then remapped onto a Mercator projection using orbital ephemeris and an automated adjustment method to correct for residual navigation errors (Bordes, Brunel, & Marsouin, 1992). To investigate seasonal, monthly and interannual variability for the period 1987 to 1999, monthly composite AVHRR SST data were obtained from the NASA Pathfinder project (Vazquez, Hamilton, Van Tran, & Sumagaysay, 1994): these data are mapped onto an equal–angle projection giving a latitudinal and longitudinal resolution of 9.8km and 7.3km at 42ºN.

2.4.2. Ocean colour

Ocean colour data were obtained from the NASA Sea–viewing Wide Field–of–view Sensor (SeaWiFS) launched in August 1997 an operational instrument that has provided daily high resolution ~1.1 km coverage over the Iberian Peninsula. Individual passes were supplied in level 1 format by the Dundee Satellite Receiving Station and analysed using the SeaWiFS Automated Processing System (SeaAPS: Lavender and Groom, 1999). SeaAPS automatically applies NASA algorithms to perform calibration, navigation images and atmospheric correction (Gordon and Wang, 1995). Images of water leaving radiance are then used to compute chlorophyll concentration with the OC4 algorithm (O'Reilly, Maritorena, Mitchell, Siegel, Carder, Garver, Kahru, & McClain, 1998) or combined to produce near–true colour images that can show scattering and absorption in the 555, 510 and 443 nm bands (Lavender & Groom, 1999). Finally, the SeaWiFS images are remapped to the same Mercator projection as the AVHRR data. SeaWiFS monthly composites on an equal–angle projection with 9.8km/7.3km pixel size (at 42ºN) were obtained from the NASA Goddard Distributed Active Archive Center to investigate the monthly and interannual characteristics of chlorophyll in the study area.

2.5. Plankton counts and estimation of primary production from P–E curves

Plankton samples were collected from 3–8 depths in the upper 100m and preserved in Lugol's iodine. The organisms were identified and counted to the species level where possible using an inverted microscope and composite sedimentation chambers. Small species (< 20µm) were counted in single transects at ×250 and ×400 while a scan of the whole slide at ×100 was used for larger species. Although inverted microscope counts cover the nano– (2–20µm) and plankton (20–200µm) size ranges, the preservation procedure could have caused losses in the nanoplankton fraction, which is mainly composed by flagellates. In addition, the picoplankton fraction (< 2µm) is not considered with this counting technique. The count data for GALICIA–XII and MORENA–I cruises provided information on horizontal distributions of plankton species, whilst vertical distribution data are available from selected transects (see **Fig. 1**) for the GALICIA–XII, MORENA–II, CD110b, MORENA–I and Bg9815c cruises.

Photosynthesis–irradiance (P–E) relationships were determined at 3 to 5 depths in the water column during cruises GALICIA–XII, CD110b, MORENA–I and Bg9815c. Sampling depths were selected on the basis of the Chl–fluorecescence profiles obtained with a fluorometer attached to the rosette sampler. Where a deep chlorophyll maximum (DCM) was observed, one sample was taken in the maximum, two samples from the upper and lower tails of the DCM, together with one sample from the surface and one sample from the 1%PAR. The P–E experiments were conducted in linear incubators illuminated at the front by tungsten halogen lamps. Each incubator housed fourteen subsamples held in 75ml tissue culture Corning flasks, inoculated with 185 kBq (5 μCi) of ^{14}C–labelled bicarbonate. The incubators were cooled with circulating surface water. The photosynthetic available radiation (E_{PAR}) at the position of each incubation bottle was measured with a Li–Cor cosine sensor LI–190SA. The flask at the end of the incubator was covered with aluminium foil and used as a measure of dark fixation. After 2–3 hours of incubation, samples were filtered through 25mm glass fibre filters (Whatman GF/F) and were exposed to concentrated HCl fumes for 12 hours. Radioactivity was determined using the external standard and the channel ratio methods to correct for quenching. The P–E parameters were estimated by fitting the data to the model of Platt, Gallegos & Harrison (1980). Water column primary production was integrated to a depth equivalent to 0.1% of surface irradiance using the P–E parameters, the chlorophyll concentration in the water column, the daily incident light and the vertical attenuation coefficient. Incident sea surface photosynthetic active radiation (PAR 400–700 nm) was measured with a Li–Cor cosine sensor (LI–190SA) and light penetration in the water column was determined using a Li–Cor spherical quantum sensor LI–193SA. Underwater PAR just below the sea surface was calculated by adjusting the PAR profile to the equation of light attenuation with depth. Light transmittance at the air–sea interface was calculated by dividing PAR light just below the sea surface by incident PAR at the sea surface.

3. Results and discussion

3.1. Wind stress patterns off NW Spain

Following Bakun & Nelson (1991), the distribution of wind–stress curl near the NW coast of the Iberian Peninsula is irregular and of low value during fall and winter, but becomes strongly cyclonic during spring and summer. Therefore, this factor is unlikely to be important in controlling the onset of the **PCCC** and simple wind–stress calculations in the 2º×2º geostrophic cell centred at 43°N 11°W (**Fig. 1c**) are adequate to define the effect of wind patterns on the seasonal reversals of the Portugal Coastal Current. Haynes & Barton (1990) observed that the weaker the equatorward wind–stress, the stronger the **PCCC** flow, while a reversal of the **PCCC** flow will only occur if the equatorward wind–stress is sufficiently strong. Consequently, a quantitative study of the recurrent modes of temporal variation of $-Q_X$ will provide information on the expected hydrographic variability on event, seasonal and inter–annual time–scales. We will focus first on seasonal variability (**section 3.1.1**), then on inter–annual variability (**section 3.1.2**), and finally on event–scale variability (**section 3.1.3**). The inter–annual variability of $-Q_X$ will be match up to AVHRR sea surface temperatures (January mean).

3.1.1. Seasonal variability: extension and intensity of the downwelling season

Retention of the 1st (T= 365 days) and 2nd (T= 183 days) harmonics of a Fourier analysis applied to the complete 1981–98 time series of $-Q_X$ values (**Fig. 2a**) produces the average seasonal cycle, SC[$-Q_X$] (**Fig. 2b**), which reveals the two well–defined periods previously noted by Wooster et al. (1976). The upwelling–favourable season (equatorward wind–stress) extends from the beginning of April to the end of September and shows a seasonal maximum of $-Q_X$ of 0.4 10^3 m^3 s^{-1} km^{-1} in July, while the downwelling–favourable season (poleward wind–stress) extends from the beginning of October to the end of March and shows a seasonal minimum of $-Q_X$ of –0.5 10^3 m^3 s^{-1} km^{-1} in December. The average period and $-Q_X$ values for the 1981–98 upwelling–favourable season are 188 days and 0.27 10^3 m^3 s^{-1} km^{-1} respectively. For the downwelling–favourable season these numbers are 177 days and –0.33 10^3 m^3 s^{-1} km^{-1}. Therefore, the average SC[$-Q_X$] is slightly biased towards downwelling–favourable values.

However, the average SC[$-Q_X$] only retains 12% of the total variability of the 1981–98 time series, pointing to a relatively low intensity of the seasonal signal. A SC[$-Q_X$] value can be produced for each individual year; these values retain from <5% in 1985–86 to >27% in 1989–90 of the total annual variability (**Table 2**).

The inter–annual variability of the monthly running mean of $-Q_X$ (**Fig. 2c**) points to **1**) a high variation in the timing of the onset and the cessation of the downwelling–favourable season each year, and **2**) the frequent occurrence of downwelling events during the upwelling season and *vice versa*. Whereas the onset of the downwelling–favourable season usually occurs from mid–September to mid–October, the cessation can extend from early February to late May. The onset of the downwelling–favourable season occurs at the time of the 'autumn phytoplankton bloom' and the subsequent period of intense organic matter degradation characteristic of temperate ecosystems (Nogueria, Pérez, & Ríos, 1997), while the time interval of cessation of the downwelling–favourable season overlaps with the period of the 'spring bloom' (Figueiras, & Niell, 1987; Nogueira et al., 1997). The occurrence/absence of the **PCCC** at the time of the spring and autumn blooms has key implications for the fate of the fresh organic materials produced during these events in the coastal zone: off–shelf export *versus in situ* sedimentation. Of particular interest are the Sept. 1991 (GALICIA–XII) cruise, during which coastal winds shifted from downwelling– to upwelling–favourable and the May 1993 (MORENA–I) cruise, when an isolated downwelling–favourable period of about 1 month occurred.

3.1.2. Decadal change of $-Q_X$ and its effect on the development of the **PCCC**

In order to highlight a possible interannual variability in the $-Q_X$ time series, it is necessary to filter the seasonal and event (high frequency) components (Fedorov, & Ovstroski, 1986). The seasonal component has been removed by subtracting the average SC[$-Q_X$] for the period 1981–98 (**Fig. 2b**) and the event component by the cumulative sums method (Ibanez, 1993). The corresponding cumulative function S[$-Q_X$] (**Fig. 2d**) is:

$$S[-Q_X(t)] = (-Q_X(t) - SC[-Q_X]) + S[-Q_X(t-1)] \quad (2)$$

where t is time in Julian day. Lower S[$-Q_X$] values indicate preferred wind conditions for **PCCC** development off the NW Iberian Peninsula. A negative (positive) trend in S[$-Q_X$] indicates transition to **PCCC** favourable (unfavourable) periods.

S[$-Q_X$] from **Figure 2d** is seen to describe a long–term cycle of T ~10 years, with minimum values (**PCCC** favourable) in the middle 80's (1984–86) and maximum values (**PCCC** unfavourable) in the middle 90's (1994–96). An abrupt S[$-Q_X$] trough during 1983 with a marked minimum in late autumn was observed, indicating that the SC[$-Q_X$] of that particular year was strongly shifted towards downwelling conditions (**Fig. 2c**). This observation accords with Pingree and Le Cann (1989), who identified a marked warming along the north Spanish coast near the New Year of 1984. Fortunately, the GALICIA–VI and GALICIA–VII cruises took place in Dec. 1983 and Feb.–Mar. 1984 respectively, allowing definition of the **PCCC** during a particularly favourable year. Wind–stress patterns in 1985 and 1989 were also exceptionally favourable to the **PCCC** development, this being reflected in the amplitude of the seasonal signal during the downwelling season 1989–90, which exhibited several $-Q_X$ minima below $-1.0\ 10^3$ $m^3\ s^{-1}\ km^{-1}$ (**Fig. 2c**). On the contrary, wind patterns during 1990 were particularly unfavourable for **PCCC** development: only a brief trough on S[$-Q_X$] was observed during the autumn. Pathfinder SST data for each January between 1987 and 1999 are shown in **Figure 3**. The **PCCC** between 42–44ºN is evident as a warming in most years, extending well into the Bay of Biscay in particular in 1990 (and 1996), with notable exceptions in 1991 (and 1994). Accordingly, an exceptional warm water anomaly (+1.5°C in the ENACW domain) was recorded by Pingree (1994) in January 1990 in the southern Bay of Biscay, which was attributed in part to the warm **PCCC** observed off Northern Spain in the winter of 1989–90. This author also indicated that there is little evidence for a marked **PCCC** in the winter of 1990–91. A marked (brief) trough on S[$-Q_X$] was observed in 1995 (1993).

Although S[$-Q_X$] during the years 1991, 1992 and 1993 was not particularly favourable for the development of the **PCCC**, it will be shown that this feature was observed during cruises GALICIA–XII (Sep. 1991), MORENA–I (May 1993) and MORENA–II (Nov.–Dec. 1993). Under these conditions, wind–stress helps to modulate the intensity of the **PCCC** which is

primarily induced by geostrophic adjustment of the weak eastward oceanic flow driven by the large–scale meridional baroclinic pressure gradient (Frouin et al., 1990). In this sense, **Figure 3** also show the average SST each January for the slope region influenced by the **PCCC** in a box 42–43ºN 9.5–10ºW. The SST variations correlate well with SST along the continental slope north of Spain between 4–8ºW from 'Centre de Meteorologie Spatiale/Centre de Meteorologie Marine' data presented in Pingree (1994: his Fig. 2) for the period of overlap (1987–1993): this is not surprising since a strong **PCCC** warming on the slope west of Spain is likely to be reflected in warming along the north coast. However, a stronger warming does not necessarily mean a stronger **PCCC** since the **PCCC** SST correlates well with average SST in an offshore region (42–43ºN; 11–13ºW; **Fig. 3**) suggesting that the interannual temperature variations are caused by larger scale forcing or that the poleward flow induced by the pressure gradient affects a much broader region.

Wind patterns changed completely during the second half of the 90's, when both the intensity and duration of the downwelling season increased. The abrupt trough on S[$-Q_X$] during 1997 demonstrated conditions to be especially favourable for the development of the **PCCC** with a marked warm water flow seen in January 1988, during cruise CD110b. Finally, a close coupling between the long–term components of a basin–scale index such as the 'North Atlantic Oscillation' (S[*NAO*]) and a meso–scale index (2º×2º) such as $-Q_X$ (S[$-Q_X$]) is clearly observed in **Figure 2c**.

3.1.3. Event scale variability

It must be highlighted that most of the variability of the $-Q_X$ time series is associated with the short–term bands of period ≤30 days (**Table 2**). The contribution of this event–scale ranges from 57% of the total variability in 1995–96 to a maximum of 79% in 1986–87, with a 1981–98 average of 66%. A significant amount of the event–scale variability (>5%, $p < 0.05$) occurs as single modes of variation with periods in the range 13 to 30 days (**Table 2**). This event–scale periodicity is a characteristic feature of the NW Spain upwelling system (Blanton, Tenore, Castillejo, Atkinson, Schwing, & Lavín, 1987; Álvarez–Salgado, Rosón, Pérez, & Pazos, 1993).

However, it should also be noted that significant modes of longer period such as 1/6 (61 days), 1/5 (73 days), 1/4 (91 days) and 1/3 (121 days) of the annual period are also apparent in certain years.

3.2. A physical framework for the PCCC off NW Spain

Geopotential anomaly, temperature and salinity distributions are analysed in this section merely with the aim of setting the framework necessary to appreciate the chemical and biological features generated by the **PCCC** off NW Spain (42º–43ºN) rather than contributing to the profuse knowledge on the physics of this structure. The distributions allow to examine the geostrophic velocity fields (**section 3.2.1**) and the geometry (**section 3.2.2)** of the **PCCC** —defined by the convergence and divergence fronts observed from the satellite images— under the contrasting conditions of the seven cruises used in the paper. In addition, a marked seasonal cycle of stratification/mixing in the **PCCC** domain is also described for the first time (**section 3.2.3**).

3.2.1. Intensity of the **PCCC** as deduced from geopotential anomaly fields

The Sep. 1991 cruise was carried out at the time of the autumn transition from upwelling– to downwelling–favourable coastal winds. The monthly running mean of $-Q_X$ (**Fig. 2c**) indicates that the cruise occurred in a low wind–stress period ($-Q_X$ = +90±50 $m^3\ s^{-1}\ km^{-1}$) after weak downwelling–favourable winds during the previous week. At the start of the cruise, winds (ship measurements) were from a westerly direction (stns 11 to 65; average 4.5 m s^{-1}) but by the end of the cruise they had swung round to a northerly direction (stns 71 to 85; average 5 m s^{-1}). As a result of the variable wind pattern, the geopotential anomaly at 10 dbar (**Fig. 4a**) was quite patchy, with alternation of poleward flow off the northern coast, equatorward flow off the western coast, and off–shelf flow adjacent to the transitional Cape Finisterre transect (43ºN). Southward geostrophic surface flows along the chosen stns 81–85 transect (**Fig. 1**) were very weak over the shelf (2 cm s^{-1}) but slightly stronger at the slope (4.5 cm s^{-1}), consistent with hydrographic conditions expected for a transitional wind–calm period at the time of the onset of the **PCCC**.

PCCC–favourable southerly wind conditions ($-Q_X$ <0) prevailed during the late autumn (Dec. 1983 and Nov.–Dec. 1993) and early winter (Jan. 1998) cruises (**Fig. 2c**). Winds (ship measurements) during the Dec. 1983 cruise were from a southerly quarter with average speed of 6.2 m s^{-1}. Strong northward geostrophic surface currents were observed across the southernmost transect from 11ºW (–11ºE) to the coast, with average and maximum velocities of 4 cm s^{-1} and 10 cm s^{-1} respectively. The **PCCC** current narrows in the vicinity of Cape Finisterre and exhibits maximum geostrophic velocities of 10 cm s^{-1} (**Fig. 4b**). In contrast, a weak (average speed, 3 cm s^{-1}) southward flowing current (the Portugal current) is observed in the north western corner of the Dec. 1983 sampling domain (stns 7 and 10). Similar values were calculated by Frouin et al. (1990) along 42ºN during the MEDPOR/2 cruise (Nov. 29 to Dec. 6, 1983). Winds during the Nov.–Dec. 1993 cruise were also **PCCC**–favourable (average speed 7.0 m s^{-1}) with poleward directed geostrophic current of average speed 6 cm s^{-1} being observed east of 10ºW (–10ºE) along 41º45'N (**Fig. 4c**). As also observed during the Dec. 1983 cruise, the current narrowed towards the north. Also of note during this cruise was the zonal entry of oceanic waters at 41ºN marked by the 4.0 m^2 s^{-2} isoline. Strong southerly winds (average speed 15 m s^{-1}) during the Jan. 1998 cruise, allowed sampling at only 5 sampling stations (**Fig. 1**). However, the presence of a strong poleward geostrophic current of about 13 cm s^{-1} on the shelf was identified (**Fig. 4d**).

As indicated in **section 3.1**, the late winter cruise (Feb.–Mar. 1984) was carried out during a period of upwelling–favourable winds within the downwelling season. The average±SD monthly running mean of $-Q_X$ was 185±160 m^3 s^{-1} km^{-1} while the mean wind velocity during the cruise was 8.2 m s^{-1}, from the north–east. As a consequence, weak north–eastward geostrophic currents dominated the study area, with maximum velocities of 2.5 cm s^{-1} (**Fig. 4e**). These conditions may be compared with the monthly running mean of $-Q_X$ (–190±100 m^3 s^{-1} km^{-1}; **Fig. 2c**) and the prevailing **PCCC**–favourable winds (south–westerly, average speed 6.3 m s^{-1}) during the spring cruise in May 1993. The surface geostrophic flow (**Fig. 4f**) clearly shows the zonal entry of the **PCCC** at 41ºN and its north–eastward progression, with a mean velocity of 2.5 cm s^{-1} near Cape Finisterre. A weak signal of the Portugal Current is also

observed offshore in the NW corner of the sampling area with southward geostrophic velocities of ~1 cm s^{-1}. The **PCCC** was also observed during April 1982 (McClain, Chao, Atkinson, Blanton, & de Castillejo, 1986), April 1987 (Bode et al., 1990), May 1989 (Mazé et al., 1997) and May 1993 (Fiúza et al., 1998). Therefore, the presence of the **PCCC** off Portugal and NW Spain during the spring appears to be a predominant hydrographic feature.

As expected, during the summer cruise in Jun.–Jul. 1998, meteorological and hydrographic conditions were very different. The average±SD monthly mean of $-Q_X$ was 390±40 m^3 s^{-1} km^{-1} with an average wind velocity during the cruise (ship measurement) of 12 m s^{-1} from the north–east, these conditions being typical of steady and strong upwelling. Accordingly, geostrophic flow calculations (**Fig. 4g**) indicated strong southward geostrophic currents, with an average southward velocity of 5 cm s^{-1} in the study area and maximum values of ~10 cm s^{-1} along 42º 9'N, off the Ría de Vigo.

3.2.2. Oceanic and coastal boundaries of the **PCCC**

The presence of poleward flowing slope currents in oceanic eastern boundaries is usually accompanied by a clear thermohaline signal resulting from the transport of anomalously warm and salty waters (Mooers, 1989). In our case, the **PCCC** conveys surface and central waters of subtropical origin (σ_0< 27.0 kg m^{-3}) to the study region. The AVHRR images (**Fig. 1**) and the horizontal distributions of surface salinity (**Fig. 5**) show the **PCCC** as an elongated high temperature and salinity core occupying the coastal transition zone (CTZ) off NW Iberian Peninsula.

Satellite imagery (**Fig. 3**) indicates the presence of thermal fronts at the coastal and oceanic boundaries of the **PCCC**. A band or patches of cool water adjacent to the west coast is separated from warmer **PCCC** waters over the continental slope by a marked convergence front. There is however, marked interannual variability with marked fronts in 1987, 1990, 1991, 1996, and 1997; in other years there are only small patches of cooling such as 1992 or the complete absence (such as 1989 at 42ºN). The front produces the accumulation of low salinity and cold waters on the shelf due to discharge from the Rías Baixas, four large coastal inlets off NW

Spain that receive continental waters from a 7×10^3 km^2 drainage basin (**Fig. 1**). The 1987–96 average seasonal cycle of continental runoff to the Rías Baixas shows an increase from 35 l s^{-1} km^{-2} in September to 70 l s^{-1} km^{-2} in November followed by a decrease to 63 l s^{-1} km^{-2} in January and 40 l s^{-1} km^{-2} in May (Nogueira et al., 1997). In agreement with the seasonal pattern, the salinity gradient is especially pronounced during late autumn and early winter (**Fig. 5d**). During the early autumn (Sep. 1991; **Fig. 5a**) and spring (May 1993; **Fig. 5f**), the inshore salinity gradient was less pronounced and the front appeared along the shelf break, strongly related to the bottom topography (Haynes & Barton, 1990; Bode et al., 1990; Fiúza et al., 1998). The coastal band of cold water (**Fig. 1**) develops in late autumn, when the whole water column begins to cool as a result of net heat loss from the surface (Fiúza, 1984; Pérez, et al., 1998). The coastward penetration of the **PCCC** depends on the relative intensity of shelf winds and that of local continental runoff that activates the residual circulation pattern of the Rías Baixas. A recent study by Álvarez–Salgado, Gago, Miguez, Gilcoto, and Pérez (2000) demonstrates that penetration of **PCCC** waters into the Rías Baixas occurs when $Q_X / R \geq 7(\pm 2)$, with Q_X in units of m^3 s^{-1} km^{-1} and R (continental runoff) in units of m^3 s^{-1}. The oceanwards boundary of the **PCCC** is characterised by a more diffuse divergence front separating the subtropical water associated with the **PCCC** from the surrounding fresher and colder open ocean water coming from the north. This front is apparent in the AVHRR sea surface temperature (SST) images (**Fig. 1**) and in the horizontal distributions of salinity in the NW corner of the survey box for the Dec. 1983, Feb.–Mar. 1984, May 1993 and Nov.–Dec. 1993 cruises (**Figs. 5b,c, e and f**).

Comparison of **Figures 5b** (Dec. 1983) and **5e** (Feb.–Mar. 1984) indicates a stronger and better–defined poleward flow in December (SSS> 35.7 at 42–43ºN) than in February (SSS< 35.7). This anomaly is probably related to the stratification conditions and the dominance of strong southerly winds in Dec. 1983 while winter mixing conditions and weak northerly winds were recorded in Feb.–Mar. 1984 as reflected in the geopotential anomaly fields (**Figs. 5b & e**). The poleward flows of May 1993 (**Fig. 5f**) and Nov.–Dec. 1993 (**Fig. 5c**) also showed differences. The high salinity core of the **PCCC** penetrated from offshore near 41ºN during the late spring cruise while during the late autumn cruise two branches of the **PCCC** could be

identified: a north–eastward flowing branch, which was also observed during the spring cruise (at 41ºN), and a northward–flowing branch on the southern side of the study area (at 40ºN). This structure is consistent with the calculated geostrophic flows (**Fig. 4c and f**) and is indicative of a southward displacement of the origin of the **PCCC** through the year (Álvarez–Salgado et al., 1993).

3.2.3. Vertical structure of the **PCCC**: a seasonal cycle of stratification/mixing

A subsurface high salinity (>35.9) core centred around 50–100m depth was observed at the slope stations during the early autumn (Sept. 91; **Fig. 6a**), late autumn (Dec. 83 and Nov.–Dec. 93, **Figs. 6b and c**), late spring (May 93; **Fig. 6f**) and summer (Jun.– Jul. 98; **Fig. 6g**). A corresponding V–shape of the isotherms occurs in the vicinity of the high salinity core during the periods of the onset (**Fig. 7a**) and cessation (**Fig. 7f**) of the **PCCC**. The presence of the core during the early autumn is a consequence of the transitional upwelling/downwelling favourable conditions recurrently observed at these particular times and indicates the presence of previously upwelled ENACW over the shelf, where it is confined by the **PCCC**. During the downwelling–favourable late autumn and early winter cruises (**Fig. 7b, c, and d**) the isotherms slope downwards in the onshore direction, intercepting the bottom at the shelf–break. The same structure is retained during the slightly upwelling–favourable late winter cruise (**Fig. 7e**) and reflects at depth the corresponding convergence front between coastal and **PCCC** waters observed in the surface layer. During the summer cruise, the isotherms slope upwards in the inshore direction (**Fig. 7g**), indicating vigorous upwelling of ENACW with the high salinity core (**Fig. 6g**) tracing the northward displacement of the summer Portugal Coastal Under–Current (Batteen, Martinez, Bryan, & Buch, 2000).

The subsurface salinity maximum develops in late spring, when a very shallow thermocline overlies the deeper remnants of the saltier mixed layer of ENACW from the previous winter (Fiúza et al., 1998). The salinity difference between the surface and the high salinity core is <0.1 at this time (**Fig. 6f**). The high salinity core is maintained beneath the seasonal thermocline during the summer (**Fig. 6g**) and early autumn (**Fig. 6a**) and surfaces from late autumn to late

winter in the **PCCC** domain (**Fig. 7c, d and e**), in tandem with the increased mixing conditions in the surface layer. Thus, upper mixed layer depth in the **PCCC** domain increased from 20m in early autumn (with maximum surface temperatures >20ºC), to 60m in late autumn (SST> 15.5ºC), to 125m in early winter (SST <15ºC) and to 150m in late winter (SST<14ºC). The situation in Dec. 1983 (**Figs. 6b and 7b**) was exceptional, with temperatures >17ºC over the upper mixed layer and a marked subsurface salinity maximum, which contrasted with the temperature of 15ºC over the 60m thick mixed layer in Nov. 1993. As indicated in **section 3.1**, the wind field in 1983–84 was especially favourable for the development of the **PCCC**, whilst it was unfavourable in 1993–94 (**Fig. 2d**).

3.3. New insights on the effects of the PCCC on the distributions of chemical parameters

Horizontal and vertical distributions of selected chemical tracers show the imprint of the **PCCC** in the coastal, transitional and oceanic waters off NW Spain. The **PCCC** domain is characterised by low surface nutrient concentrations compared with the surrounding coastal and oceanic waters. Relatively high carbon and nutrients and low oxygen concentrations were observed in the ENACW domain as a consequence of oceanic mineralisation (**section 3.3.1**) and nitrite is revealed as a tracer of stratification/mixing conditions and associated trophic status of the **PCCC** (**section 3.3.2**).

The convergence front between the **PCCC** and coastal waters results in a reduction of the off–shelf export of primary production, thus enhancing *in situ* sedimentation and pelagic/benthic mineralisation processes on the shelf which, in turn, will affect carbon, nutrient and oxygen distributions. In contrast, the divergent front between the **PCCC** and the surrounding oceanic water creates local upwelling, enhancing vertical fluxes of nutrients to the nitrogen–exhausted surface layer. Since nutrient enrichment of shelf bottom waters has been the subject of specific papers (Álvarez–Salgado et al., 1993; Álvarez–Salgado et al. 1997; Prego & Bao, 1997), we just want to show here that vertical distributions of NO_3^- (**Fig. 9**) indicate substantial nutrient enrichment in shelf bottom waters, in comparison with ENACW of the same temperature in the surrounding ocean. The effect was specially intense during the onset (**Fig.**

9a) of the **PCCC**, when NO_3^- concentrations of 13º–13.5ºC water increased from <7 μmol kg^{-1} in the ocean domain to >11 μmol kg^{-1} over the shelf. Nutrient enrichment in bottom shelf waters was also important during the late autumn cruise (Nov.–Dec. 1993; **Fig. 9c**), the late winter cruise (Feb.–Mar. 1984; **Fig. 9e**) and during the cessation of the **PCCC** (May 1993; **Fig. 9f**). In contrast, nutrient–poor **PCCC** waters occupied the bottom inner shelf during Jan. 1998 (**Fig. 9d**). During Jun.–Jul. 1998 the parallelism between temperature (**Fig. 7g**) and NO_3^- profiles (**Fig. 9g**) indicates reduced nutrient enrichment during strong upwelling events.

Horizontal distributions of NO_3^- (**Fig. 8**) show relatively high nutrient concentrations in the surface layer of the coastal domain during the late autumn (Dec. 1983) and early winter (Jan. 1998) cruises due to accumulation of nutrient–rich low–salinity (**Figs. 5 and 6**) continental waters discharged from the Rías Baixas (Pérez, Álvarez–Salgado, Rosón & Ríos, 1992). Surface nutrients in the coastal domain were very low (<0.2 μmol kg^{-1} NO_3^-) during the onset (Sep. 1991; **Fig. 8a**) and cessation (May 1993; **Fig. 8f**) of the **PCCC**. Conversely, increased nutrient concentrations observed on the southern side of the coastal domain during the Nov.–Dec. 1993 cruise (**Fig. 8c**) resulted from intense vertical mixing and entrainment of nutrient–rich deeper waters rather than from land runoff, as indicated by the high salinity of the surface waters (**Fig. 5c**) and the homogeneous vertical profiles of the thermohaline and of the chemical tracers at stns 72 and 73 (not shown). High surface nutrient concentrations during the summer cruise (Jun.–July 1998), mainly observed in the Cape Finisterre area (>6 μmol kg^{-1} NO_3^-), were due to upwelling, as indicated by the low SST in the coastal domain (**Fig. 1**). Vertical NO_3^- profiles (**Fig. 9**) supports this conclusion. It is remarkable also that weak salinity stratification of coastal waters during the Feb.–Mar. 1984 cruise (**Fig. 6e**) kept NO_3^- concentrations below those recorded in the vigorously mixed **PCCC** and oceanic waters (**Fig. 9e**).

3.3.1. Chemistry of surface and central waters transported by the **PCCC**

The principal attribute of the subtropical surface waters transported by the **PCCC** to the Eastern North Atlantic temperate/subpolar transition area is the low nutrient concentrations compared to either the adjacent coastal and oceanic waters, as clearly shown by the surface

(**Fig. 8**) and vertical (**Fig. 9**) distributions of NO_3^-. The effect on nutrient distributions of the divergent front in juxtaposition to the oceanic waters is clearly evident in the relatively high surface nutrients in the NW corner of the Nov.–Dec. 93 (**Fig. 8c**) and May 93 (**Fig. 8f**) cruises. Surface NO_3^- concentrations in the **PCCC** domain were usually <0.5 μmol kg^{-1}, except during the winter mixing period (125–150m mixed layer) when concentrations of 1.5–2.0 μmol kg^{-1} were recorded. For comparison, surface NO_3^- concentrations were >4 μmol kg^{-1} in the oceanic domain west of the **PCCC** flow. These low NO_3^- values in the surface waters of the **PCCC** have important implications for the extension of the spring bloom. Assuming a Chl–*a* production to NO_3^- consumption ratio of 1:1 (the theoretical maximum for phytoplankton of Redfield composition; Anderson, 1995), Chl–*a* levels at the time of the spring bloom will never exceed 2 mg m^{-3} in the **PCCC** domain. Evidence supporting this comes from the SeaWiFS monthly composites for 1998, 1999 and 2000 (not shown): in a region influenced by the **PCCC** (40.5–41.5ºN, 9.5–11ºW) the spring chlorophyll maximum is ~1 mg m^{-3}. It is also important to note that there are HPO_4^{2-} and SiO_4H_4 excesses of 0.03–0.04 μmol kg^{-1} and 0.5–1.5 μmol kg^{-1}, respectively, for NO_3^- <0.1 μmol kg^{-1} (not shown), suggesting that nitrogen is the limiting nutrient to primary production in surface **PCCC** waters.

Apparent oxygen utilisation (AOU) can be used as an indicator of the balance of physical (net exchange across the air–sea interface) and biogeochemical (production/mineralisation) processes operating in surface **PCCC** waters. Primary production is the dominant process contributing to AOU during the onset of the **PCCC** (Sept. 91 cruise), inducing average AOU values of –10 μmol kg^{-1} (not shown). For comparison, AOU of the order of –40 μmol kg^{-1} was recorded in the coastal domain. These numbers agree with the primary production rates recorded during the Sept. 91 cruise, which were 4–6 times higher in the coastal than in the **PCCC** domain (**section 3.4.3**). **PCCC** waters were at oxygen equilibrium with the atmosphere (–1.0< AOU < 2.0 μmol kg^{-1}) during the late autumn and early winter cruises, most probably because of the low primary production (**section 3.4.3**) and enhanced air–sea exchange (intense coastal winds, **section 2.2**). At this time, slight regeneration was observed in the coastal domain, where the average AOU was +8 μmol kg^{-1}. During the late winter cruise, weak mineralisation dominated

in the **PCCC** domain (average AOU, +4 μmol kg^{-1}) but intense primary production occurred in the coastal domain (average AOU, –30 μmol kg^{-1}), suggesting that the spring bloom had taken place in coastal waters off NW Spain by that time. Very variable AOU values, ranging from –5 to –20 μmol kg^{-1}, were observed both in the **PCCC** and in the coastal domains during the late spring cruise.

In our analysis of the chemical features of ENACW transported by the **PCCC**, seawater samples between the shallow ENACWst salinity maximum at 26.6–26.8σ_0 (50–100m depth) and the deep ENACWsp salinity minimum at 27.2σ_0 (450–500m depth) have been selected from the set of sampling stations in the area defined by parallels 42º and 43ºN, and meridian 11ºW (–11ºE) and the 1000m isobath. Data from the sampling stations inshore of the 1000m isobath have been rejected owing to the effect of shelf mineralisation processes on the nutrient–temperature relationships of ENACW. A total of 395 samples have been considered.

The resulting θ/*S* diagram (not shown) exhibits the expected positive linear relationship between temperature and salinity (r= +0.94 **Table 3**), with ENACW temperatures ranging from 10.5 to 15ºC. The standard error of the salinity (±0.05) or temperature (±0.4ºC) estimates from the θ/*S* regression are of the order of magnitude of the variability observed for ENACW by Pérez et al. (1995). These authors found a decadal cycle of salinity/temperature changes of ENACW in parallel to the decadal changes of $-Q_X$ (**Fig. 2d**). Accordingly, a clear salinity excess of +0.05 and/or temperature deficit of –0.4ºC was observed at the time of GALICIA–XII (1991), and MORENA–I and –II (1993) compared with the GALICIA–VI and –VII (1983–84) and the CD110b and Bg9815c (1998).

The chemical characteristics of ENACW transported by the **PCCC** have been studied by regression analysis of the selected samples above . C_T, nitrate and phosphate show a significant negative correlation with temperature through the ENACW domain (r< –0.89; **Table 3**). C_T is normalised to salinity 35.0 and corrected of calcium carbonate precipitation–dissolution (NC_Tcor) by subtracting –0.5×(NTA+NO_3), according to Broecker and Peng (1982). It was found that a quadratic regression model better explained the silicate–temperature relationship

(r= –0.94), indicating that ENACWsp is silicate–richer than ENACWst. This maybe expected from the higher silica fluxes in subpolar than in subtropical waters (Nelson, Treguer, Brzezinski, Leynaert, & Queguiner, 1995). The regression was lower in the case of the AOU of ENACW transported by the **PCCC** (r= –0.82). Álvarez–Salgado, Beloso, Joint, Nogueira, Chou, Pérez, Groom, Cabanas, Rees & Elskens (submitted) have recently pointed out that the nutrient anomalies of the regressions with temperature (ΔNO_3^-, ΔHPO_4^{2-} and ΔSiO_4H_4) are not significantly correlated with the corresponding salinity anomalies (ΔS; $r < 0.20$), suggesting that nutrient anomalies are not due to the observed decadal changes in the thermohaline properties of ENACW. Our study confirms a similar observation for the AOU and NC_Tcor anomalies (ΔAOU and ΔNC_Tcor). Assuming that temperature removes the effect of ENACW mixing, then the ΔAOU, ΔNC_Tcor, ΔNO_3^-, ΔHPO_4^{2-} and ΔSiO_4H_4 variability must result from biogeochemical processes. Thus, carbon and nutrient anomalies were well correlated, with a C/N/P molar ratio of 108±12/16.7±0.6/1 (**Table 3**), indicating that the anomalies were due to the rapid mineralisation of sinking organic particles of Redfield composition (Anderson and Sarmiento, 1994). Silicate and nitrate anomalies were also well correlated (r = +0.79), with a N/Si molar ratio of 2.4±0.1. Following the Redfield ratios observed in carbon and nutrient anomalies, a $\Delta AOU/\Delta NO_3^-$ ratio of 9–10 mol O_2 mol N^{-1} would be expected. However, despite the relatively high correlation between AOU and nitrate anomalies (r= +0.92), the O_2/N molar ratio was only 6.8±0.2; that is about 70% of the expected Redfield value. This would seem to result from the study area being within the North Atlantic ventilated thermocline where the ENACWsp forms (Castro, Pérez, Holey, & Ríos, 1998). As a consequence, AOU levels in the cold and nutrient–rich ENACWsp branch are much lower than expected from the carbon and nutrient distributions due to intense ventilation of the water mass just off the study area, where mixed layer depths may exceed 500m.

3.3.2. Seasonal development of nitrite profiles in relation to the stratification/mixing sequence of **PCCC** waters

Nitrite (NO_2^-) profiles at the time of the onset of the **PCCC** (**Fig. 10a**) were characterised in the coastal domain by a small subsurface maximum of ~0.10 μmol kg^{-1} at the base of the nutricline (**Fig. 9a**). Nitrite was undetectable (<0.02 μmol kg^{-1}) above and below the subsurface maximum. This structure was still observed in late autumn during the anomalous **PCCC**–favourable situation of the Dec. 1983 cruise (**Fig. 10b**). Moreover, relatively high NO_2^- levels were observed in the surface mixed layer of both the coastal (>0.2 μmol kg^{-1}) and the **PCCC** (0.05–0.10 μmol kg^{-1}) domains during **PCCC**–unfavourable years, such as during the Nov.–Dec. 1993 cruise (**Fig. 10c**). Surface mixed layer NO_2^- levels in the **PCCC** domain increased to ~0.15 μmol kg^{-1} during the Jan. 1998 cruise and ~0.25 μmol kg^{-1} during the Feb.–Mar. 1984 cruise. The increase of NO_2^- from late autumn to late winter in the **PCCC** domain parallels to the progressive deepening of the winter mixed layer from 60m (Nov.–Dec. 1993) to 125m (Jan. 1998) and to 150m (Feb.–Mar. 1984). Surface mixed layer NO_3^- concentration (**Fig. 9c, d and e**) also increased in parallel with the one of NO_2^-. The subsurface NO_2^- maximum re–forms again during spring, in both the coastal and the **PCCC** domains, with high values (>0.20 μmol kg^{-1}) present at the nitracline (**Fig. 10f**). In contrast, an intrusion of saline water with high NO_2^- (~0.20 μmol kg^{-1}) was observed at the Cantabrian shelf–break (Bay of Biscay), in April 1987 (Bode et al., 1990), resembling the structure observed off 42º–43ºN during the winter. This suggests that the **PCCC** off the Bay of Biscay in spring retains the mixing conditions observed off the western coast during the winter. During the summer (Jun.–Jul. 1998), the subsurface NO_2^- maximum is very weak when the poleward flow is represented only by the undercurrent (**Fig. 10g**).

A subsurface NO_2^- maximum is a common feature of N–limited oligotrophic systems, where it is usually referred to as the 'primary nitrite maximum' (PNM; Wada & Hattori, 1991). A PNM is observed in shelf waters off NW Spain during the relaxation periods between consecutive upwelling pulses throughout the upwelling–favourable season, when the system switches from meso– to oligotrophic conditions (Figueiras & Ríos, 1993). The feature is also

observed in the adjacent stratified and N–exhausted oceanic waters (Castro, Pérez, Álvarez–Salgado, & Fraga, 2000), generally being found at the 'level of no motion' between the southward flowing surface layer and the northward flowing Portugal Coastal Under Current (Batteen et al., 2000).

Enhanced light inhibition of bacterial oxidation of NO_2^- to NO_3^- compared with NH_4^+ oxidation to NO_2^- is commonly cited as the main reason for the formation of the PNM in oligotrophic waters (Olson 1981a; Wada & Hattori, 1991; Dore & Karl 1996). Therefore, the presence of the PNM during the autumn and spring cruises could be explained by the oligotrophic waters of subtropical origin conveyed by the **PCCC** to temperate/subpolar latitudes. However, the large NO_2^- excess observed in the **PCCC** surface mixed layer during the winter cruises when NO_3^- concentrations are relatively high (>1.5 μmol kg^{-1}) is not present under oligotrophic conditions. Liberation of NO_2^- from phytoplankton during assimilative NO_3^- reduction has been documented (Vaccaro & Ryther, 1960; Kiefer et al. 1976; Olson, 1981b; Dore & Karl, 1996) with the amount of NO_2^- produced varying inversely with the intensity of light. This is consistent with the observed increase of NO_2^- concentration in parallel to surface mixed layer deepening through the winter. Therefore, it seems that under these low–light conditions, phytoplankton are able to efficiently reduce NO_3^- to NO_2^- while the conversion of NO_2^- to NH_4^+ (which requires much more energy and reduction power) becomes the limiting step in the NO_3^- assimilatory pathway (Blasco, 1971). It should be noted that the phytoplankton species in the NW Iberian margin are adapted to the winter light conditions, but the maximum production per unit of Chl–*a*, P_m^B = 1.4±0.4 gC (g Chl–*a*)$^{-1}$ h^{-1}, is less than 1/3 of the summer values (see **section 3.4.3**; **Table 4**), which should affect their energy and reduction–power resources. This phytogenic hypothesis is not contradictory with NO_2^- release by active bacterial regeneration (Wada & Hattori, 1991) and/or grazing by microflagellates on bacteria, which also enhance the release of NO_2^- to the water column (Rault, Sohier, Rivier & Daumas, 1988).

3.4. New insights on the effects of the PCCC on the distributions of biological parameters

Horizontal and vertical distributions of Chl–*a* and key plankton taxa illustrate the biological consequences of the onset, development and cessation of the **PCCC** off NW Spain. High Chl–*a* concentrations, created primarily by large diatoms and dinoflagellates, were observed on the shelf, whereas low Chl–*a* concentrations, associated particularly with small plankton forms, predominated in **PCCC** waters, with a higher proportion of small flagellates during winter and small dinoflagellates, mainly *Gymnodinium* spp., during autumn (**section 3.4.1**). Shelf–edge exchange of plankton species is prevented by the convergent front created by the **PCCC** on the slope, such that coastal diatoms were totally absent in the **PCCC** domain (**section 3.4.2**). Enhanced sedimentation of coastal plankton over the shelf contributed substantially to the observed nutrient enrichment of shelf bottom waters. Plankton biomass carried by the **PCCC** exhibited less production rates than the plankton present in the coastal waters during the autumn, whereas primary production was higher in **PCCC** than in shelf waters during late spring. The photosynthetic parameters and the depth of the photic layer are invoked to explain the differences observed in the productivity of **PCCC** and of coastal phytoplankton (**section 3.4.3**).

3.4.1. Effect of the **PCCC** on the Chl–*a* distributions

Over 1000 individual SeaWiFS passes from September 1997 to January 2001 were analysed to produce synoptic chlorophyll and ocean colour fields for the western Iberian Peninsula. In order to describe the ocean colour characteristics of the **PCCC** and surrounding shelf and oceanic waters, a sequence of four clear images from October 1997 and January, February and March 1998 was selected for two reasons: first, the only cruise described herein to sample the **PCCC** subsequent to the launch of SeaWiFS took place in January 1998; second, the **PCCC** in winter of 1997/8 exhibited a distinct signal in the SST data. The SeaWiFS data are presented in **Figure 11**, along with the corresponding SST. **Figure 11a** is the SST of 29 October 1997: a distinct warm band, the **PCCC**, can be seen extending off the western coast, turning right at Cape Finisterre to enter the Cantabrian Sea. As a consequence of the convergence created by the

warm band, high levels of Chl–a accumulated along the coast, which contrasted with the oligotrophic condition in the PCCC and surrounding oceanic waters (**Fig. 11b**). On 21 January 1998 (at the end of the CD110b cruise) the warm band had extended into the Cantabrian sea and an anticyclonic eddy had formed north of Cape Ortegal (**Fig. 11c**). This feature is similar in location to a slope water oceanic eddy (swoddy) visible in satellite data presented by Pingree and Le Cann (1990). The chlorophyll image (**Fig. 11d**) shows high concentrations over the shelf associated with a cooler band of water, with distinct front along the 200m contour and as far as the 2000m at 42.4–43ºN. However, the colour composite (**Fig 11e**) shows that the chlorophyll retrieval on the shelf is affected by high scattering probably due to suspended particulate matter associated with river–runoff and absorption by coloured dissolved organic matter: **Figure 12d** notes an *in situ* chlorophyll value of 0.85 mg m^{-3} from CD110b compared to ~2.2 mg m^{-3} SeaWIFS estimate at the same location, albeit 6 days later. Hence, care must be taken interpreting winter estimates of chlorophyll on the shelf. The **PCCC**, in contrast with the SST, does not exhibit a distinct signal in the ocean colour data south of 42ºN. Peliz and Fiúza (1999) noted that the **PCCC** would appear distinct from shelf or oceanic waters if it possessed a distinct colour signature, related to different levels of chlorophyll: during winter the chlorophyll field is relatively uniform off–shelf with higher concentrations on the shelf.

One month later, on 24 February 1998, the **PCCC** SST signature (**Fig. 11f**) was similar in appearance to the January image and SeaWiFS (**Fig. 11g**) again shows elevated chlorophyll on the shelf. In contrast to January, the colour composite (not shown) exhibits absorption as opposed to scattering suggesting that the enhanced chlorophyll is associated with phytoplankton growth. There was a sharp front aligned with the coast extending over the 200m contour and coincident with cooler coastal water. The chlorophyll concentration dropped sharply across the front from ~1.7 mg m^{-3} to 0.45 mg m^{-3} at 43ºN. Chlorophyll concentration within the **PCCC** appeared slightly higher than waters further offshore. The SST image appeared to show a second warm '**PCCC**–like' band extending northward between 12–13ºW 40–41ºN.

Figures 11h and i comprise SST and chlorophyll data for 24 March 1998. The warming associated with the **PCCC** was no longer pronounced north of 43ºN and the SST at 43.5ºN

9.2ºW has decreased from 15.5ºC in January, 14.7ºC in February and 14.1ºC in March. There was elevated chlorophyll in a narrow band along the coast, and offshore of 11ºW between 41º–43ºN the latter suggesting the start of the spring bloom. Between the shelf and offshore waters there was a low chlorophyll wedge associated with the warmer SST of the **PCCC**. This feature was observed by Peliz and Fiúza (1999) on individual CZCS images in spring (typically in May) and on monthly composite images for May and October/November. The appearance in March 1998 is explained by Joint et al. (2002) who analysed SeaWiFS images for the region and suggested that the Spring bloom occurred earlier in 1998 than 1999; a similar earlier appearance also occurred in March 2000. The low chlorophyll wedge was visible on SeaWiFS monthly composites including March and October 1998 and May and October 1999 (see **Figures 11j and k).**

Aside from the synoptic view provided by the selected SeaWIFS images, Chl–*a* was measured during the cruises utilized in this paper. Surface Chl–*a* distributions for these cruises (**Fig. 12**) show that the main consequence of the low chlorophyll **PCCC** in the NW Iberian margin was its ability to restrict coastal plankton to the shelf region. The influence was marked during early autumn (Sep. 1991, **Fig. 12a**), late autumn (Nov.–Dec. 1993, **Fig. 12c**) and late winter (Feb.–Mar. 1984, **Fig. 12e**) rather than during the middle winter (Jan. 1998, **Fig. 12d**) and late spring (May 1993, **Fig.12f**) due to higher Chl–*a* concentrations in coastal waters during the former than during the latter cruises. Although retention of the coastal 'autumn bloom' on the shelf at the time of the onset of the **PCCC** has been previously described by Castro et al. (1997) in September 1986, the corresponding confinement of the coastal 'spring bloom' is described here for the first time (**Fig. 12e**). The convergence front created by the **PCCC** favours the sedimentation and benthic mineralisation of the 'spring bloom' materials formed in the shelf waters of the NW Iberian margin rather than its off–shelf export. Contrary to what may be expected for an upwelling system, the co–ocurrence of the 'spring bloom' and the **PCCC**, would produce intense recycling of the new primary production in the coastal domain. The Chl–*a* distribution in Feb.–Mar. 1984 presents a good example of the difference between 'new' and 'export' production. This observation has important implications in relation to the potential

capacity of coastal upwelling systems to absorb atmospheric CO_2. If the new production of the spring bloom is recycled rather than exported, then, the net effect of the biological CO_2 pump is nil. Although, to our knowledge, similar conditions have not been described for other coastal upwelling systems, it would seem likely that they may occur in hydrographically comparable areas.

Low surface Chl–*a* concentrations on the shelf during the early winter and late spring cruises (**Fig. 12d and f**) were caused by the strong mixing conditions encountered during the winter (**Fig 7d**), which reduce phytoplankton concentrations in the mixed layer, and by the low surface nutrient concentrations during late spring (**Figs. 8f and 9f**), which limit phytoplankton growth. In contrast, during the upwelling season (**Fig. 12g**), high chlorophyll values were recorded (>7 mg m^{-3} off the Rías Baixas) with the surface distribution suggesting an off–shelf export of this fresh material.

The vertical distributions of Chl–*a* (**Fig. 13**) confirmed that the highest concentrations were located over the shelf, also revealing the presence of a subsurface chlorophyll maximum located at ~50m, from the cessation (late spring, May 1993) to the onset (early autumn, Sep. 1991) of the **PCCC**. The subsurface chlorophyll maximum, which extended from the shelf break to the open ocean waters, coincided with the presence of stratified oceanic surface waters (**Fig. 7**) and low mixed layer nutrient concentrations (NO_3^- <0.5 μmol kg^{-1}; **Fig. 9**) in the area. In contrast, the stronger vertical mixing conditions during the period of maximum **PCCC** development (Jan. 1998; **Fig. 13d**) determined the quasi–homogenous distribution of Chl–*a* over the surface 100–150m. High Chl–*a* concentrations in shelf surface waters and a subsurface maximum in the adjacent stratified ocean waters, are typical of coastal upwelling systems (e.g. Basterretxea & Arístegui, 2000). Chl–*a* concentrations in the subsurface maximum (>0.5 mg m^{-3}, **Figs. 12a and g**) were similar to values recorded in other mesotrophic areas, such as the Kuroshio Current off Japan (Takahashi, Nakai, Ishimaru, Hasumoto & Fijita, 1985), the western Mediterranean (Estrada, 1985) and the off–shelf waters of the NW African upwelling system (Basterretxea & Arístegui, 2000). We also note that the relatively high Chl–*a* concentrations in the deep upper

mixed layer (>100m) of the **PCCC** domain during the winter produced integrated water column Chl–*a* concentrations greater than observed during the spring, summer and autumn (**Table 4**).

3.4.2. Isolation of **PCCC** from coastal plankton species

The action of the **PCCC** in restricting the shelf–edge exchange of materials also has a marked effect on the distribution of plankton numbers in the study area during the onset (Sep. 1991) of the **PCCC**, when the autumn bloom exported from the Rías Baixas (diatom numbers >2000 cell ml^{-1};**Fig. 14f**), was confined in the shelf. Accumulation on the shelf of dinoflagellates (**Fig. 14k**) and flagellates (**Fig. 14p**) also occurred during this cruise. In this sense, when southerly winds become strong but rainfall is still limited (high Q_X/R ratio), meteorological conditions that could occur at the beginning of the autumn, the **PCCC** can favours dinoflagellate blooms, sometimes of toxic species, inside the Rias Baixas. It has been argued that these blooms may develop either selection of species already present in the interior of the Rias Baixas (e.g. Figueiras, Jones, Mosquera, Álvarez–Salgado, Edwards & MacDougall, 1994) or by entrainment of oceanic phytoplankton assemblages (e.g. Fraga, Bravo & Reguera, 1993).

The late autumn (Nov.–Dec. 1993) and winter (Jan. 1998) cruises showed vertically homogeneous plankton distributions, with a strong dominance of small flagellates (**Figs. 14b & c, and 14 q & r**), but and almost complete absence of diatoms (**Figs. 14g & h**) and dinoflagellates (**Figs. 15l & m**). Unfortunately, no samples were available from the surface waters of the coastal stations during the Nov.–Dec. 1993 cruise, where a Chl–*a* maximum of 3 mg m^{-3} was found (**Fig. 13c**). Small flagellates were more abundant at the westernmost oceanic stations during both cruises, confirming that winter **PCCC** waters are associated with mainly this phytoplankton grouping. Small flagellates were also dominant in **PCCC** waters during the May 1993 cruise (**Figs. 14d & s**) while dinoflagellates (small *Gymnodinium* spp.) were also relatively important (**Fig. 14n**). The most striking feature of the late spring **PCCC** event, as deduced from the vertical distributions, was the confinement of diatoms to the narrow band of

coastal waters (**Fig. 14i**). Sedimentation of the diatoms is favoured at the convergence adjacent to the slope.

Diatoms were also confined in coastal waters during upwelling in Jun.–Jul. 1998 (**Fig. 14j**), whereas dinoflagellates were exported further offshore (**Fig. 14o**) in the surface layer. In contrast, the subsurface Chl–*a* maximum at 50m (**Fig. 14e**) was constituted primarily by small flagellates (**Fig. 14t**). The swimming capacity of dinoflagellates allows them to remain in the surface layer during off–shelf export, whereas diatoms are able to sediment out of the stratified waters. Diatoms are able to remain in the surface layer only in well–mixed water columns as occur during upwelling. During a recent Lagrangian study of the off–shelf export of materials produced in the upwelling centre of Cape Finisterre, mediated through the Rías Baixas filament described by Haynes et al. (1993), Joint et al. (2001) recorded a similar situation with the diatoms being confined on the shelf but the dinoflagellates being exported by the filament.

3.4.3. Primary production rates in **PCCC** and coastal waters

Primary production (*PP*; **Table 4**) in coastal waters confined by the **PCCC** was higher during early autumn (Sep. 1991; 2.1±0.71 gC m^{-2} d^{-1}) than during late spring (May 1993; 0.4±0.11 gC m^{-2} d^{-1}) despite the fact that integrated Chl–*a* levels and photic–layer depths being similar during the two cruises (**Table 4**). The day length was longer in the less–productive spring period (15h) than during the autumn cruise (11h), indicating that the difference was caused by the higher maximum photosynthetic rate (P_m^B) of phytoplankton populations advected from Rías Baixas during the Sep. 1991 cruise. In contrast, *PP* rates in the **PCCC** domain were higher during late spring (0.78±0.3 gC m^{-2} d^{-1}) than in the autumn (0.4±0.13 gC m^{-2} d^{-1}). Since the comparable values of P_m^B were similar in this instance (p = 0.55), the higher *PP* in late spring is likely to be due to the longer day–length and the slightly deeper photic layer at this time. Photosynthetic efficiency (α^B) of the phytoplankton in the **PCCC** waters during the May 1993 cruise was higher than during the Sep. 1991cruise (p <0.01) and, consequently, the light saturation parameter E_k was lower in the May 1993 late spring cruise. This indicates

that photosynthesis was light saturated at lower irradiances in late spring than in autumn and, this may partially explain the higher *PP* in spring.

PP in **PCCC** waters was low during the winter (Jan. 1998; 0.14±0.044 gC m^{-2} d^{-1}) despite the phytoplankton populations being low–light adapted (E_k = 41±13 μmol m^{-2} s^{-1}) and the integrated Chl–*a* being higher than during autumn and late spring **PCCC** events (**Table 4**). The reason for the low winter *PP* appears to be the extremely low P_m^B = 1.4±0.4 gC (gChl–*a*)$^{-1}$ h^{-1}. The low–light adaptation of photosynthesis in the **PCCC** waters in winter reflects the strong mixing of the water column (~125m), which was deeper than the photic layer, implying that the average light received by the phytoplankton was low. In addition, as indicated in **section 3.3.2**, insufficient P_m^B rates were available to meet the energy and reduction–power requirements to efficiently reduce NO_2^- to NH_4^+, inducing the accumulation of NO_2^- in the upper mixed layer (**Fig. 10d**).

Recently upwelled coastal waters in summer (Jun.–Jul. 1998, **Table 4**) showed *PP* not substantially different from those of confined coastal waters in autumn (Sep. 1991). Low maximum photosynthetic rates (P_m^B) contributed significantly to the low *PP* since integrated Chl–*a* concentrations were significantly higher in summer than in autumn. However, *PP* in the oceanic stratified waters in summer was between the autumn and late spring values. It would seem likely that the lower E_k of the oceanic waters compared to the **PCCC** waters accounted for the higher *PP* in summer, since integrated Chl–*a* in the photic layer and P_m^B at this time were similar. The lower E_k values indicate that photosynthesis was light saturated at lower irradiance values during summer than in autumn. In late spring *PP* was higher in **PCCC** waters than in summer stratified waters due to the higher integrated Chl–*a* concentrations in the photic layer; here P_m^B and E_k values were not significantly different between cruises ($0.51 < p < 0.53$).

PP values reported in the present study compare favourably with the monthly–average satellite–derived production rates of the **PCCC** domain in this area presented by Joint, Groom, Wollast, Chou, Tilstone, Figueiras, Loijens, Smyth (in press). In any case, it should be noted

that these authors have used part of the *PP* data of this paper (those of the Jun.–Jul. 1998 and Jan. 1998 cruises) to produce their satellite–derived estimates. Teira, Serret & Fernández (2001) have reported *PP* rates for the October 1998 **PCCC** conditions. Their average value of 491±65 mg C m^{-2} d^{-1} compares very well with our value of 356±134 mg C m^{-2} d^{-1} during Sep. 1991 (**Table 4**). Values in the coastal domain during Jun.–Jul 1998 (2.1 g C m^{-2} d^{-1}, **Table 4**) should be considered as the lower limit of possible *PP* rates during the upwelling season. Values ranging from 3.2 to 7.4 g C m^{-2} d^{-1} have been reported by Teira et al. (2001) and, exceptionally, as much as 10 g C m^{-2} d^{-1} have been measured in shelf waters off the Rías Baixas during the 'spring bloom' by F.G. Figueiras (unpubl.). Discarding extremely high 'spring bloom' and extremely low winter values (0.14 g C m^{-2} d^{-1}; **Table 4**), the range of *PP* rates off NW Spain was similar to those recorded in the Benguela (0.5–4 g C m^{-2} d^{-1}; Brown & Field, 1986; Estrada & Marrasé, 1987; Brown, Painting & Cochraine, 1991), the Peru (1.9 g C m^{-2} d^{-1}; Barber & Smith, 1981) and the California (0.5–2.6 g C m^{-2} d^{-1}; Pilskan, Paduan, Chavez, Anderson & Berelson, 1996) coastal upwelling systems.

4. Summaries and major conclusions

Combination of available wind–stress data, satellite–derived sea surface temperature and chlorophyll distributions and hydrographic data collected during seven cruises off the NW Iberian margin together with comparable published information have allowed us to study the effects of the Portugal Coastal Counter Current on the chemistry and biology of the NW Iberian margin during the understudied downwelling–favourable season (September– May), when the Portugal Coastal Counter Current (**PCCC**) develops. Summaries of the novel contributions of this paper to the knowledge of the **PCCC** are listed below.

1) <u>On the modes of variability of the coastal winds off NW Spain</u>: alongshore coastal wind–stress, a major modulating agent of the direction and intensity of the coastal circulation, exhibits a remarkable short–time–scale variability, with 66% of it (average 1982–98) concentrated on periods ≤30 days. The seasonal cycle of upwelling–favourable winds, from the beginning of April to the end of September, and downwelling–favourable winds, the rest

of the year, only explains from <5% to >27% of the coastal wind variability (1982–98 average, 12%). The onset of the downwelling–favourable season use to concentrate from mid September to mid October, at the time of the autumn plankton bloom, whereas the cessation can occur from early February to late May, coinciding, or not, with the spring plankton bloom. Marked interannual variability is observed from 1982 to 1998, describing a long–term cycle of ~10 year period, in association to the basin–scale North Atlantic Oscillation, which clearly defines **PCCC** favourable and unfavourable years.

2) On the stratification/homogenisation cycle in **PCCC** waters: The warm and salty surface and central waters transported by the **PCCC** experience a marked seasonal cycle of stratification/homogenisation, with upper mixed layer depths gradually increasing from 20m in late summer–early autumn, 60m in late autumn, 125m in early winter to 150m in late winter. This cycle has important implications for the chemistry and biology of **PCCC** waters.

3) On the seasonal evolution of nitrite profiles in PCCC waters: it is remarkable the seasonal progression of nitrite in **PCCC** waters in relation to the stratification/homogenisation cycle. A brief subsurface maximum <0.1μmol kg^{-1} is observed during the early autumn. It evolves to a marked winter mixed layer maximum of >0.2 μmol kg^{-1}, which changes to a subsurface maximum of >0.2 μmol kg^{-1} during the spring. As supported below (point 6), we are more inclined for a 'phytogenic' rather than a 'bacteriogenic' hypothesis for the development of the nitrite maximum during the winter.

4) On the stoichiometry of mineralization in ENACW conveyed by the PCCC: ENACW transported by the **PCCC** is nutrient enriched by intense mineralization processes during poleward displacement. O_2/C/N/P mineralisation ratios results to be not significantly different from the Redfield values characteristic of the early degradation of the products of phytoplankton photosynthesis.

5) On the separation of **PCCC** and coastal plankton populations under downwelling conditions: the downwelling front created on the shelf by the **PCCC** separates two contrasting environments. On one hand, the mesotrophic conditions in the coastal domain due to **1**) the

nutrient–rich continental waters discharged from the Rías Baixas and accumulated on the shelf during the winter or **2**) intense nutrient mineralisation processes at the sediment–water interface during the spring and autumn. On the other hand, oligotrophic conditions (<0.1 μmol kg^{-1} NO_3^-) are observed in the stratified, <20m deep, spring and autumn surface mixed layer of the **PCCC**, whereas higher nutrient levels (>1.0 μmol kg^{-1} NO_3^-) occur in the >100m deep winter mixed layer. The front is usually located at the slope, except during periods of strong southerly winds and/or limited runoff, when the **PCCC** invades the shelf and even enters the rías. Small flagellate forms dominate the plankton assemblages of **PCCC** waters, which are clearly differentiated from large plankton forms (diatoms and dinoflagellates) of coastal waters. The **PCCC** confines coastal plankton on the shelf. This effect is especially important at the time of the spring and autumn blooms. In this sense, the seasonal cycle of surface Chl–*a* in the Ría de Vigo reveals that maximum concentrations (>7 mg m^{-3}) are recorded during May and September (Nogueira et al., 1997), that is at the time of the onset and cessation of the **PCCC,** respectively. Therefore, intense **PCCC** events at these particular times of the year will favour the *in situ* mineralisation of sinking organic matter, mainly diatoms, produced at high rates in the rías–shelf system.

6) <u>On the photosynthesis response of PCCC and coastal plankton populations to downwelling conditions</u>: primary production of coastal waters during the downwelling–favourable season depends on the seasonal evolution of the maximum photosynthetic rate (P_m^B), which is highest during autumn. Photic layer depth and day length are the two factors which determine that primary production in **PCCC** waters is higher during spring than in autumn. Although Chl–*a* concentrations are higher in winter than during autumn and spring, primary production rates in **PCCC** waters are extremely low during the winter because of the low P_m^B values. The low P_m^B could be responsible for the large NO_2^- accumulation in the winter mixed layer because the energy and reduction–power obtained during phytoplankton photosynthesis could be not enough to satisfy the requirements for carbon fixation and reduction of NO_2^- to NH_4^+.

5. Acknowledgements

The authors wish to thank the Captain, crew and technicians of Research Vessels 'García del Cid' (GALICIA–VI and –VII), 'Investigador S.' (GALICIA–XII), 'Cornide de Saavedra' (MORENA–I), 'Hakon Mosby' (MORENA–II), 'Charles Darwin' (CD110b) and 'Belgica' (Bg9815c) for their help during the sampling programme. J. M. Cabanas (IEO, Vigo) has provided the Ekman transport data. T. Rellán helped with the preparation of figures. These cruises were performed with the financial support of the CICYT grant No. MAR97−2068−CE and the EU contract numbers MAS1–CT90–0017 ('The Control of Phytoplankton Dominance') MAS2–CT93–0065 ('MORENA') and MAS3–CT97–0076 (OMEX II–II).

6. References

Álvarez–Salgado, X.A., Pérez, F.F., & Fraga, F. (1992). Determination of nutrient salts by automatic methods both in seawater and brackish water: the phosphate blank. *Marine Chemistry, 39*, 311–319.

Álvarez–Salgado, X.A., Rosón, G., Pérez, F.F., & Pazos, Y. (1993). Hydrographic variability off the Rías Baixas (NW Spain) during the upwelling season. *Journal of Geophysical. Research, 98*, 14447–14455.

Álvarez–Salgado, X.A., Castro, C.G., Pérez, F.F., & Fraga, F. (1997). Nutrient mineralization patterns in shelf waters of the Western Iberian upwelling. *Continental Shelf Research, 17*, 1247–1270.

Álvarez–Salgado, X.A., Gago, J., Miguez, B.M., Gilcoto, M., & Pérez, F.F. (2000). Surface waters of the NW Iberian upwelling system: upwelling on the shelf versus outwelling of upwelled waters from the Rías Baixas. *Estuarine, Coastal & Shelf Science*, *51*, 821–837.

Álvarez–Salgado, X.A., Beloso, S., Joint, I., Nogueira, E., Chou, L., Pérez, F.F., Groom, S., Cabanas, J.M., Rees, A., & Elskens, M. (submitted). New production of the NW Iberian shelf during the upwelling season. *Deep–Sea Research, part I*

Ambar, I., Fiúza, A.F.G., Boyd, T., & Frouin, R. (1986). Observations of a warm oceanic current flowing northward along the coasts of Portugal and Spain during November–December 1983. *EOS transactions, American Geophysical Union*, *67(44)*, 1054.

Ambar, I., & Fiúza, A.F.G. (1994). Some features of the Portugal Current System: a poleward slope undercurrent, an upwelling–related summer southward flow and an autumn–winter poleward coastal surface current. In: *Proceedings of the second International Conference on Air–Sea Interaction and on Meteorology and Oceanography of the Coastal Zone*, K.B. Katsaros, A.F.G. Fiúza, & I. Ambar, editors, American Meteorological Society, pp. 286–287.

Anderson, L.A. (1995). On the hydrogen and oxygen content of marine phytoplankton. *Deep–Sea Research I, 42*, 1675–1680.

Anderson, L.A., & Sarmiento, J.L. (1994). Redfield ratios of remineralization determined by nutrient data analysis, *Global Biogeochemical Cycles*, *8*, 65–80

Arhan, M., Colin de Verdière, A., & Memery, L. (1994). The eastern boundary of the subtropical North Atlantic. *Journal of Physical Oceanography*, *24*, 1295–1316.

Bakun, A. (1973). Coastal upwelling indices, west coast of North America, 1946–71, NOAA Technical Report NMFS–671, 103 pp.

Bakun, A., & Nelson, C.S. (1991). The seasonal cycle of wind–stress curl in subtropical eastern boundary current regions. *Journal of Physical Oceanography*, *21*, 1815–1834.

Barber, R.T., & Smith, R.L. (1981). Coastal Upwelling Ecosystems. In: *Analysis of marine ecosystems*, Longhurst, A.R., editor, Academic press, New York, pp 31–68.

Barton, E.D. (1989). The poleward undercurrent on the eastern boundary of the subtropical North Atlantic. In: *Poleward Flows along Ocean Eastern Boundaries, Coastal and Estuarine Studies,* Vol. 34, S.J. Neshyba, Ch.N.K. Moores, R.L. Smith, & R.T. Barber, editors, Spinger–Verlag, pp. 82–92.

Barton, E.D., & 21 authors more (1998). The transition zone of the Canary Current upwelling region. *Progress in Oceanography, 41*, 455–504.

Basterretxea, G., & Arístegui, J. (2000). Mesoscale variability in phytoplankton biomass distribution and photosynthetic parameters in the Canary–NW African coastal transition zone. *Marine Ecology Progress Series*, *197*, 27–40.

Batteen, M.L:, Martinez, J.R., Bryan, D.W., & Buch, E.J. (2000). A modeling study of the coastal eastern boundary current system off Iberia and Morocco. *Journal of Geophysical Research*, *105*, 14137–14195.

Blanton, J.O., Tenore, K.R., Castillejo, F.F., Atkinson, L.P., Schwing, F.B, & Lavín, A. (1987). The relationship of upwelling to mussel production in the rías on the western coast of Spain. *Journal of Marine Research*, *45*, 497–511.

Blasco, D. (1971). *Acumulación de nitritos en determinados niveles marinos por acción del fitoplancton*. Doctoral Thesis, University of Barcelona, 223 pp.

Bode, A., Fernández, E., Botas, A., & Anadón R. (1990). Distribution and composition of suspended particulate matter related to shelf–break saline intrusion in the Cantabrian Sea (Bay of Biscay). *Oceanologica Acta*, *13*, 219–228.

Bordes, P., Brunel, P., & Marsouin, A. (1992). Automatic adjustment of AVHRR navigation. *Journal of Atmospheric and Oceanic Technology*, *9*, 15–27.

Borges, A.V., & Frankignoulle, M. (2002). Aspects of dissolved inorganic carbon dynamics in the upwelling system off the Galician coast. *Journal of Marine Systems*, *32*, 181–198.

Brink, K.H., & Cowles, T.J. (1991). The coastal transition zone program. *Journal of Geophysical Research, 96*, 14367−14648.

Broecker, W.S., & Peng, T.–H (1982). *Tracers in the Sea*, Eldigio Press, New York, 690 pp.

Brown, P.C., &Field, J.G. (1986). factors limiting phytoplankton production in a nearshore upwelling area. *Journal of Plankton Research*, *8*, 55–68.

Brown, P.C., Painting, S.J., & Cochraine, K.L. (1991). Estimates of phytoplankton and bacterial biomass and production in the northern and southern Benguela ecosystems. *South African Journal Marine Science*, 11, 537–564.

Castro, C.G., Álvarez–Salgado, X.A., Figueiras, F.G., Pérez, F.F., & Fraga, F. (1997). Transient hydrographic and chemical conditions affecting microplankton populations in the coastal transition zone of the Iberian upwelling system (NW Spain) in September 1986. *Journal of Marine Research*, *55*, 321–352.

Castro, C,G., Pérez, F.F., Holey, S.E. & Ríos, A.F. (1998). Chemical characterisation and modelling of water masses in the North East Atlantic. *Progress in Oceanography*, *41*, 249–279.

Castro, C.G., Pérez, F.F., Álvarez–Salgado, X.A., & Fraga, F. (2000). Coupling between thermohaline and chemical fields during two contrasting upwelling events off the NW Iberian Peninsula. *Continental Shelf Research*, *20*, 189–210.

Church, J.A., Cresswell, G.R., & Godfrey, J.S. (1989). The Leewin Current. In: *Poleward Flows along Ocean Eastern Boundaries, Coastal and Estuarine Studies,* Vol. 34, S.J. Neshyba, Ch.N.K. Moores, R.L. Smith, & R.T. Barber, editors, Spinger–Verlag, pp. 230–252.

Cresswell, G.R., & Golding, T.J. (1980). Observation of a south flowing current in the Southeastern Indian Ocean. *Deep Sea Research*, *27*, 449–466.

Dickson, A.G. (1993). pH buffers for sea water media based on the total hydrogen ion concentration scale. *Deep–Sea Research I, 40,* 107–118.

Dore, J.E., & Karl, D.M: (1996). Nitrite distributions and dynamics at Station ALOHA. *Deep–Sea Research, part II, 43*, 385–402.

Estrada, M. (1985). Deep phytoplankton and chlorophyll maxima in the Western Mediterranean. In: *Mediterranean Marine Ecosystems*, M. Moraitou–Apostolopulou, & V. Kiortsis, editors, Plenum Press, New York, pp 247–277.

Estrada, M., Marrasé, C. (1987). Phytoplankton biomass and productivity off the Namibian coast. In : *The Benguela and Comparable Ecosystems*, A.I.L. Payne, J.A. Gulland, & K.H. Brink, editors, *South African Journal Marine Science*, *5*, 347–356.

Fernández, E., Bode, A., Botas, A., & Anadon, R. (1991). Microplankton assemblages associated with saline fronts during a spring bloom in the central Cantabrian Sea: differences in trophic structure between water bodies. *Journal of Plankton Research*, *13*, 1239–1256.

Figueiras, F.G., & Niell, F.X. (1987). Composición del fitoplancton en la ría de Pontevedra (NO de España). *Investigación Pesquera, 51,* 371–409.

Figueiras, F.G., & Ríos, A.F. (1993). Phytoplankton succession, red tides and hydrographic regime in the Rías Bajas of Galicia. In: *Toxic Marine Phytoplankton*, T.J. Smayda, & Y. Shimizu, editors, Elsevier, New York, pp. 239–244.

Figueiras, F.G., Jones, K., Mosquera, A.M., Álvarez–Salgado, X.A., Edwards, A., & MacDougall, N. (1994). Red tide assemblage formation in an estuarine upwelling ecosystem: Ría de Vigo. *Journal of Plankton Research 16*, 857–878.

Fiúza, A.F.G. (1984). Hidrologia e dinâmica das aguas costeiras de Portugal. Ph D. Thesis, University of Lisbon, 294 pp.

Fiúza, A.F.G., Hamann, M., Ambar, I., Diaz del Río, G., González, N., & Cabanas, J.M. (1998). Water masses and their circulation off western Iberia during May 1993. *Deep–Sea Research I, 45*, 1127–1160.

Fraga, S., Bravo, I., & Reguera, B. (1993). Poleward surface current at the shelf break and blooms of *Gymnodinium catenatum* in Ria de Vigo (NW Spain). In: *Toxic Phytoplankton Blooms in the Sea*, T. J. Smayda & Y. Shimizu, editors , Elsevier, pp. 245–249.

Freeland, H.J. (1989). Observations of the low–frequency circulation off the west coast of British Columbia, Canada. In: *Poleward Flows along Ocean Eastern Boundaries, Coastal and Estuarine Studies,* Vol. 34, S.J. Neshyba, Ch.N.K. Moores, R.L. Smith, & R.T. Barber, editors, Spinger–Verlag, pp. 132–139.

Frouin, R., Fiúza, A.F.G., Ambar, I., & Boyd, T.J. (1990). Observations of a poleward surface current off the coasts of Portugal and Spain during winter. *Journal of Geophysical Research*, *95*, 679–691.

Hansen, H.P., Grasshoff, K. (1983). Automated chemical analysis. In: *Methods of seawater analysis*, 2nd Edition. K. Grasshoff, M. Ehrhardt, K. Kermling, editors, Verlag Chemie, Wheinheim, pp. 347–395

Haynes, R., & Barton, E.D. (1990). A poleward flow along the Atlantic coast of the Iberian Peninsula. *Journal of Geophysical Research*, *95*, 11425–11441.

Haynes, R., & Barton, E.D. (1991). Lagrangian observations in the Iberian Coastal Transition Zone. *Journal of Geophysical. Research*, *96*, 14731–14741.

Hidy, G.M. (1972). A view of recent air–sea interaction research. *Bulletin of the American Meteorological. Society*, *53*, 1083–1102.

Huthnance, J.M. (1995). Circulation, exchange and water masses at the ocean margin: the role of physical processes at the shelf edge. *Progress in Oceanography*, *35*, 353–431.

Huyer, A., Kosro, P.M., Lentz, S.J., & Beardsley, R.C. (1989). Poleward flow in the California Current System. In: *Poleward Flows along Ocean Eastern Boundaries, Coastal and Estuarine Studies,* Vol. 34, S.J. Neshyba, Ch.N.K. Moores, R.L. Smith, & R.T. Barber, editors, Spinger–Verlag, pp. 142–156.

Ibanez, F., Dauvin, J.C., & Ettienne, M. (1993). Comparison des evolutions à long –term (1977–1990) de deux peuplements macrobenthiques de la bahie de Morlaix (Manche Occidentale): relations avec les facteurs hycroclimatiques. *Journal of the Experimental Marine Biology and Ecology*, *16*, 181–214.

Joint, I., Groom, S., Wollast, R., Chou, L., Tilstone, G.H., Figueiras, F.G., Loijens, M., Smyth T.J., in press. The response of phytoplankton production to periodic upwelling and relaxation events at the Iberian shelf break: estimates by the ^{14}C method and by satellite remote sensing. *Journal of Marine Systems*

Joint, I., Inall, M., Torres–Almarza, R., Figueiras, F.G., Álvarez–Salgado, X.A., & Woodward, M. (2001). Two lagrangian Experiments in the Iberian Upwelling System: tracking an upwelling event and an off–shore filament. *Progress in Oceanography, 51,* 221–248.

Kiefer, D.A., Olson, R.J., & Holm–Hansen, O. (1976) Another look at the nitrite and chlorophyll maxima in the central North Pacific. *Deep–Sea Research*, *23*, 1199 – 1208.

Krauss, W., & Käse, R. (1984). Mean circulation and eddy kinetic energy in the Eastern North Atlantic. *Journal of Geophysical Research*, *89*, 3407–3415.

Lavender, S.J., and Groom, S. B. (1999). The SeaWiFS Automatic Data Processing System (SeaAPS). *International Journal of Remote Sensing*, *20*, 1051–1056.

Lavín, A., Díaz del Río, G., Cabanas, J.M., & Casas, G. (1991). Afloramiento en el noroeste de la península Ibérica. Indices de afloramiento para el punto 43 grados N y 11 grados W periodo 1966–1989. *InformesTécnicos del Instituto Español de Oceanografía* **91**. 40pp.

Mazé, J.P., Arhan, M., & Mercier., H. (1997). Volume budget of the eastern boundary layer off the Iberian Peninsula. *Deep–Sea Research I*, *44*, 1543–1574.

McClain E.P., W.G. Pichel, and C.C. Walton (1985). Comparative performance of AVHRR–based multichannel sea–surface temperatures. *Journal of Geophysical Research, 90*, 11587–11601.

McLain, C.R., Chao, S.–Y., Atkinson, L.P., Blanton, J.O., & de Castillejo, F.F. (1986). Wind–driven upwelling in the vicinity of Cape Finisterre. *Journal of Geophysical Research*, *91*, 8470–8486.

McCreary, J.P., Shetye, S.R., & Kundu, P.J. (1986). Thermohaline forcing of eastern boundary currents with application to the circulation off the west coast of Australia. *Journal of Marine Research, 44*, 71–92.

Miller, P., Groom, S., McManus, A., Selley, J. & Mironnet, N. (1997). PANORAMA: a semi–automated AVHRR and CZCS system for observation of coastal and ocean processes. RSS97: Observations and Interactions, In: *Proceedings of the Remote Sensing Society*, pp 539–544, Reading, September 1997.

Mooers, C.N.K. (1989). Workshop summary: poleward flow–observational and theoretical issues. In: *Poleward Flows along Ocean Eastern Boundaries, Coastal and Estuarine Studies,* Vol. 34, S.J. Neshyba, Ch.N.K. Moores, R.L. Smith, & R.T. Barber, editors, Spinger–Verlag, pp. 2–16.

Mouriño, C., & Fraga, F. (1985). Determinación de nitratos en agua de mar. *Investigación Pesquera*, *49*, 81–96.

Nelson, D.M., Treguer, P., Brzezinski, M., Leynaert, A. & Queguiner, B. (1995). Production and dissolution of biogenic silica in the ocean: revised global estimates, comparison with regional data and relationship to biogenic sedimentation. *Global Biogeochemical Cycles*, *8*, 359–372.

Nogueira, E., Pérez, F.F., & Ríos, A.F. (1997). Seasonal patterns and long–term trends in an estuarine upwelling ecosystem (Ría de Vigo, NW Spain). *Estuarine, Coastal and Shelf Science, 44*, 285–300.

Olson, R.J. (1981a). Differential photoinhibiton of marine nitrifying bacteria: a possible mechanism for the formation of the primary nitrite maximum. *Journal of Marine Research*, *39*, 227–238.

Olson, R.J. (1981b). ^{15}N Tracer studies of the primary nitrite maximum. *Journal of Marine Research*, *39*, 203–225.

O'Reilly, J.E., Maritorena, S., Mitchell, B.G., Siegel, D.A., Carder, K.L., Garver, S.A., Kahru, M., & McClain, C. (1998) Ocean color chlorophyll algorithms for SeaWiFS. *Journal of Geophysical Research*, *103*, 24937–24953.

Pelíz, A.J., & Fiúza, A.F.G. (1999). Temporal and spatial variability of CZCS–derived phytoplankton pigment concentration off the western Iberian Peninsula. *International Journal of Remote Sensing*, *20***,** 1363–1403.

Pérez F.F., Álvarez–Salgado, X.A., Rosón, G., & Ríos A.F. (1992). Carbonic–calcium system, nutrients and total organic nitrogen in continental runoff to the Galician Rías Baixas, NW Spain. *Oceanologica Acta, 15*, 595–602

Pérez, F. F., Ríos, A.F., King, B.A., & Pollard, R.T. (1995). Decadal changes of θ–S relationship of the Eastern North Atlantic Central Water (ENAW). *Deep–Sea Research I*, *42*, 1849–1864.

Pérez, F.F, & Fraga, F. (1987a). The pH measurements in seawater on NBS scale. *Marine Chemistry*, *21*, 315–327.

Pérez, F.F., & Fraga, F. (1987b). A precise and rapid analytical procedure for alkalinity determination. *Marine Chemistry*, *21*, 169–182.

Pérez, F.F., Castro, C.G., Álvarez–Salgado, X.A., & Ríos, A.F. (2001). Coupling between the Iberian margin scale circulation and the eastern boundary Portugal current. *Deep–Sea Research I, 48,* 1519–1533.

Pérez, F.F., Mouriño, C., Fraga, F., & Ríos, A.F. (1993). Displacement of water masses and remineralization rates off the Iberian Peninsula by nutrient anomalies. *Journal of Marine Research*, *51*, 869–892.

Pérez, F.F., Ríos, A.F., & Rosón, G. (1998). Sea Surface carbon dioxide off the Iberian Peninsula (North Eastern Atlantic Ocean). *Journal Marine Systems, 19*, 27–46.

Pérez, F.F. , Castro, C.G., Álvarez–Salgado, X.A., & Ríos, A.F. (2001). Coupling between the Iberian basin–scale circulation and the Portugal boundary current system. A chemical study. *Deep Sea Research I*, *48*, 1519–1533.

Pilskaln, C.H., Paduan, J.B., Chavez, F.P., Anderson, R.Y., & Berelson, W.M. (1996). Carbon export and regeneration in the coastal upwelling system of Monterey Bay, central California. *Journal Marine Research*, *54*, 1149–1178.

Pingree, R.D. (1993). Flow of surface waters to the west of the British Isles and in the Bay of Biscay. *Deep–Sea Research II*, *40*, 369–388.

Pingree, R.D. (1994). Winter warming in the southern Bay of Biscay and lagrangian eddy kinematics from a deep–drogued argos buoy. *Journal of the Marine Biological Association of the UK*, *74*, 107–128.

Pingree, R.D., & Le Cann, B. (1989). Celtic and Armorican slope and shelf residual currents. *Progress in Oceanography*, *23*, 303–338.

Pingree, R.D., &. Le Cann, B. (1990). Structure , strength and seasonality of the slope currents in the Bay of Biscay region., *Journal of the Marine Biological Association of the UK*, *70*, 857–885.

Pingree, R.D., Sinha, B., & Griffiths, C.R. (1999). Seasonality of the European slope current (Goban Spur) and ocean margin exchange. *Continental Shelf Research*, *19*, 929–975.

Planet W.G. (1988). *Data extraction and calibration of TIROS–N/NOAA radiometers*. NOAA Technical Memorandum NESS 107 Rev 1, Washington.

Platt, T., Gallegos, C.L., & Harrison, W.G. (1980). Photoinhibition of photosynthesis in natural assemblages of marine phytoplankton. *Journal of Marine Research*, *38*, 687–701.

Pollard, R. T., & Pu, S. (1985). Structure and circulation of the upper Atlantic Ocean northeast of the Azores. *Progress in Oceanography*, *14*, 443–462.

Poularikas, A.D., & Seely, S. (1991). *Signals and Systems*, 2nd Edition. PWS–KENT Publishing Company, Boston, 1015 pp.

Prego, R., & Bao, R. (1997). Upwelling influence on the Galician coast: silicate in shelf waters and underlying surface sediments. *Continental Shelf Research*, *17*, 307–318

Rault, P.L., Sohier, L.P., Rivier, A.M., & Daumas, R.A. (1988). Dark bacterial–protozoan culture: acidification, nitrite accumulation and protozoan inhibition in the absence of phytoplankton. *Journal of the Experimental Biology and Ecology*, *116*, 273–291.

Reid, J.L., & Mantyla, A.W. (1976). The effect of the geostrophic flow upon coastal elevations in the northern North Pacific. *Journal of Geophysical Research*, *81*, 3100–3110.

Richardson, P.L. (1983). Eddy kinetic energy in the North Atlantic from surface drifters. *Journal of Geophysical Research*, *88*, 4355–4367.

Ríos, A.F., Pérez, F.F., & Fraga, F. (1992). Water masses in upper and middle North Atlantic Ocean east of the Azores. *Deep–Sea Research I*, *39*, 645–658.

Roy R.N., Roy, L.N., Vogel, K.M., Porter–Moore, C., Pearson, T., Good, C.E., Millero, F.J., & Cambell, D.J. (1993). Determination of the ionization constants of carbonic acid in seawater in salinities 5 to 45 and temperatures 0 to 45°C. *Marine Chemistry, 44*, 249–267.

Smith, R.L. (1989). Poleward flows along eastern ocean boundaries: an introduction and historical review. In: *Poleward Flows along Ocean Eastern Boundaries, Coastal and Estuarine Studies,* Vol. 34, S.J. Neshyba, Ch.N.K. Moores, R.L. Smith, & R.T. Barber, editors, Spinger–Verlag, pp. 17–24.

Smith et al., 1991

Stevens, I., Hamann, M., Johnson, J.A., & Fiúza, A.F.G. (2000). Comparisons between a fine resolution model and observations in the Iberian shelf–slope region. *Journal of Marine Systems*, *26*, 53–74.

Swallow, J.C., Gould, W.J., & Saunders, P.M. (1977). Evidence for a poleward eastern boundary current in the North Atlantic Ocean. *ICES hydrography committee*, C.M. 1977/c:32, 21 pp.

Takahashi, M., Nakai, T., Ishimaru, T., Hasumoto, H., & Fujita, Y. (1985). Distribution of the Subsurface Chlorophyll Maximum and its Nutrient–Light Environment in and Around the Kuroshio off Japan. *Journal of the Oceanographical Society of Japan*, *41*, 73–80.

Teira, E., Serret, P., & Fernández, E. (2001). Phytoplankton size–structure, particulate and dissolved organic carbon production and oxygen fluxes through microbial communities in the NW Iberian coastal transition zone. Marine Ecology Progress Series*, 219,* 65–83.

Vaccaro, R.F., & Ryther, J.H. (1960). Marine phytoplankton and the distribution of nitrite in the sea. *Journal du Conseil Permanent International pour l'Exploration de la Mer*, *25*, 260–271.

Vázquez, J., Hamilton, M., Van Tran, A., & Sumagaysay, R.M. (1994). JPL Physical Oceanography DAAC reprocesses ten years of sea–surface temperature measurements from NOAA AVHRR. *The Earth Observer*, *6,* 16–17.

Wooster, W.S., Bakun, A., & Mclain, D.R. (1976). The seasonal upwelling cycle along the eastern boundary of the North Atlantic. *Journal of Marine Research*, *34*, 131–141.

Yentsch, C.S., & Menzel, D.W. (1963) A method for the determination of phytoplankton chlorophyll and phaeophytin by fluorescence. *Deep–Sea Research*,*10*, 221–231.

Figure captions

Figure 1. Map of the survey area (NW Iberian Peninsula) for the set of seven cruises included in this work: GALICIA–XII (Sep 1991) (**a**), GALICIA–VI (Nov–Dec 1983) (**b**), MORENA–II (Nov 1993) (**c**), CD110b (Jan 1998) (**d**), GALICIA–VII (Feb–Mar 1984) (**e**), MORENA–I (May 1993) (**f**), and Bg9815c (Jul 1998) (**g**). White points show the position of the stations occupied on each cruise. Solid lines represent the cross–shelf sections used in Figures 6, 7, 9, 10, 13 and 15. The 2º×2º geostrophic–wind cell centered at 43ºN 11ºW (–11ºE) is presented in chart **c**. The 1000 m isobath is also included. AVHRR images correspond to the sampling dates and are the most representative for the sea surface temperature distribution found during the cruises. Major Geographic features are presented in panel **c**.

Figure 2. Offshore Ekman transport values ($-Q_X$) calculated from the wind field at the 2º×2º geostrophic cell centred at 43ºN 11ºW (–11ºE) for the period August 1981 – August 1998. (**a**) Time–series of daily values of $-Q_X$ (in 10^3 m^3 s^{-1} km^{-1}) Positive (negative) values indicate upwelling (downwelling) favourable winds. (**b**) Average 1981–98 seasonal cycle of $-Q_X$, SC[$-Q_X$] (**c**) Seasonal and interannual variability of the 30–days running mean of $-Q_X$. (**d**) De–seasonalised cumulative sums of $-Q_X$ and the North Atlantic oscillation (*NAO*) index over the period 1981–98, S[$-Q_X$] and S[*NAO*] respectively. Dashed line, 1–year running mean of S[$-Q_X$].

Figure 3. AVHRR Pathfinder 9–km resolution sea–surface temperature images for each January from 1987 to 1999 (monthly composite). The 200m and 2000m depth contours are marked on each image. The white lines represent the boundaries of the **PCCC**. Bottom right panel: Extracted mean *SST* for a **PCCC** 'box' 42–43° N 9.5–10°W (± SD) and ocean box 42–43°N; 11–13°W (SD omitted for clarity).

Figure 4. Horizontal distributions of surface dynamic height (in m^2 s^{-2}) referred to 350db during the GALICIA–XII (Sep 1991) (**a**), GALICIA–VI (Nov–Dec 1983) (**b**), MORENA–II (Nov 1993) (**c**), CD110b (Jan 1998) (**d**), GALICIA–VII (Feb–Mar 1984) (**e**), MORENA–I (May 1993) (**f**), and Bg9815c (Jul 1998) (**g**) cruises. Superimposed on Figure 5c is the conversion

of distance among consecutive dynamic height isolines (separated 0.05 m^2 s^{-2}) into geostrophic velocity (cm s^{-1}).

Figure 5. Horizontal distributions of surface salinity during the GALICIA–XII (Sep 1991) (**a**), GALICIA–VI (Nov–Dec 1983) (**b**), MORENA–II (Nov 1993) (**c**), CD110b (Jan 1998) (**d**), GALICIA–VII (Feb–Mar 1984) (**e**), MORENA–I (May 1993) (**f**), and Bg9815c (Jul 1998) (**g**) cruises.

Figure 6. Vertical distributions of salinity along the zonal lines indicated in **Figure 1** during the GALICIA–XII (Sep 1991) (**a**), GALICIA–VI (Nov–Dec 1983) (**b**), MORENA–II (Nov 1993) (**c**), CD110b (Jan 1998) (**d**), GALICIA–VII (Feb–Mar 1984) (**e**), MORENA–I (May 1993) (**f**), and Bg9815c (Jul 1998) (**g**) cruises.

Figure 7. Vertical distributions of potential temperature (ºC) along the zonal lines indicated in **Figure 1** during the GALICIA–XII (Sep 1991) (**a**), GALICIA–VI (Nov–Dec 1983) (**b**), MORENA–II (Nov 1993) (**c**), CD110b (Jan 1998) (**d**), GALICIA–VII (Feb–Mar 1984) (**e**), MORENA–I (May 1993) (**f**), and Bg9815c (Jul 1998) (**g**) cruises.

Figure 8. Horizontal distributions of surface nitrate (μmol kg^{-1}) during the GALICIA–XII (Sep 91) (**a**), GALICIA–VI (Nov–Dec 1983) (**b**), MORENA–II (Nov 1993) (**c**), CD110b (Jan 1998) (**d**), GALICIA–VII (Feb–Mar 1984) (**e**), MORENA–I (May 1993) (**f**), and Bg9815c (Jul 1998) (**g**) cruises.

Figure 9. Vertical distributions of nitrate (μmol kg^{-1}) along the zonal lines indicated in **Figure 1** during the GALICIA–XII (Sep 1991) (**a**), GALICIA–VI (Nov–Dec 1983) (**b**), MORENA–II (Nov 1993) (**c**), CD110b (Jan 1998) (**d**), GALICIA–VII (Feb–Mar 1984) (**e**), MORENA–I (May 1993) (**f**), and Bg9815c (Jul 1998) (**g**) cruises.

Figure 10. Vertical distributions of nitrite (μmol kg^{-1}) along the zonal lines indicated in Figure 1 during the GALICIA–XII (Sep 1991) (**a**), GALICIA–VI (Nov–Dec 1983) (**b**), MORENA–II (Nov 1993) (**c**), CD110b (Jan 1998) (**d**), GALICIA–VII (Feb–Mar 1984) (**e**), MORENA–I (May 1993) (**f**), and Bg9815c (Jul 1998) (**g**) cruises.

Figure 11. Satellite images from: 29 October 1997, AVHRR–SST (**a**), SeaWiFS chlorophyll–a (**b**); 21 January 1998, AVHRR–SST (**c**), SeaWiFS chlorophyll–a (**d**), SeaWiFS colour

composite of 555, 510 and 443 nm bands (**e**); 25 February 1998, AVHRR–SST (**f**), SeaWiFS chl–a (**g**); 24 March 1998, AVHRR–SST (**h**), SeaWiFS chl–a (**i**). SeaWiFS monthly composites for May 1999 (**j**), and October 1999 (**k**). Note different chlorophyll–*a* scale for image h and i. The 200m and 2000m depth contours are marked on each image. AVHRR–SST in ºC and SeaWiFS chlorophyll–a in mg m^{-3}.

Figure 12. Horizontal distributions of surface chlorophyll–*a* (μg l^{-1}) during the GALICIA–XII (Sep 1991) (**a**), GALICIA–VI (Nov–Dec 1983) (**b**), MORENA–II (Nov 1993) (**c**), CD110b (Jan 1998) (**d**), GALICIA–VII (Feb–Mar 1984) (**e**), MORENA–I (May 1993) (**f**), and Bg9815c (Jul 1998) (**g**) cruises.

Figure 13. Vertical distributions of chlorophyll–*a* (mg m^{-3}) along the zonal lines indicated in **Figure 1** during the GALICIA–XII (Sep 1991) (**a**), GALICIA–VI (Nov–Dec 1983) (**b**), MORENA–II (Nov 1993) (**c**), CD110b (Jan 1998) (**d**), GALICIA–VII (Feb–Mar 1984) (**e**), MORENA–I (May 1993) (**f**), and Bg9815c (Jul 1998) (**g**) cruises.

Figure 14. Vertical distributions along the zonal lines indicated in **Figure 1** of plankton numbers (cell ml^{-1}) during the GALICIA–XII (Sep 1991) (**a**), MORENA–II (Nov 1993) (**b**), CD110b (Jan 1998) (**c**), MORENA–I (May 1993) (**d**), and Bg9815c (Jul 1998) (**e**) cruises; diatom numbers (cell ml^{-1}) during the Sep 1991 (**f**), Nov 1993 (**g**), Jan 1998 (**h**), May 1993 (**i**), and Jul 1998 (**j**) cruises; dinoflagellate numbers (cell ml^{-1}) during the Sep 1991 (**k**), Nov 1993 (**l**), Jan 1998 (**m**), May 1993 (**n**), and Jul 1998 (**o**) cruises; and flagellate numbers (cell ml^{-1}) during the Sep 1991 (**p**), Nov 1993 (**q**), Jan 1998 (**r**), May 1993 (**s**), and Jul 1998 (**t**) cruises.

Table 1. Relevant information about the cruises referred to in this study, including sampling dates, vessel, gear, measured variables and prevailing oceanographic conditions

Cruise	Dates	Vessel	Sampling Gear	Measured variables					Oceanographic Scenario	
				θ/S	Nut	Chl	Plan	PP	prevailing winds	PCCC conditions
GALICIA–VI	1–12 Dec. 1983	C. de Saavedra	Niskin bott., inv. therm.	×	×	×			Southerly, 6.2 m s^{-1}	Late autumn PCCC favour. cond.
GALICIA–VII	18 Feb.–7 Mar. 1984	C. de Saavedra	Niskin bott., inv. therm.	×	×	×			North Easterly, 8.2 m s^{-1}	Late winter PCCC favour. cond.
GALICIA–XII	10–18 Sep. 1991	Investigador S.	CTD, rosette sampler	×	×	×	×	×	Westerly, 4.5 m s^{-1}	PCCC onset
MORENA–I	10–26 May 1993	C. de Saavedra	CTD, rosette sampler	×	×	×	×	×	South Westerly, 6.3 m s^{-1}	PCCC cessation
MORENA–II	15 Nov.– 2 Dec. 1993	Hakon Mosby	CTD, rosette sampler	×	×	×	×		Southerly, 7.0 m s^{-1}	Late autumn PCCC favour. cond.
CD110b	6–16 Jan. 1998	Charles Darwin	CTD, rosette sampler	×	×	×	×	×	Southerly, 15 m s^{-1}	Early winter PCCC favour. cond.
BG9815Cc	26 Jun.–7 Jul. 1998	Belgica	CTD, rosette sampler	×	×	×	×	×	North Easterly, 12 m s^{-1}	PCCC unfavour. (upwelling favour.)

Table 2. Distribution of the temporal variance of $-Q_X$ for different years throughout the 1981–98 study period. Years are defined from August to July, such that the downwelling–favourable season is at the middle of each period. The percentage of explained variance (%E.V.) retained by the first (T = 365 days) and second (T = 183 days) harmonics of the annual period (which define the seasonal cycle, SC[$-Q_X$]), and by the short–term bands of T<30 days are indicated. The last column shows the period (%E.V.) of some significant harmonics, those with %E.V.>5% and p< 0.05, each year.

Year	**SC[$-Q_X$]**		**Short–term bands**		**Significant harmonics**
(Aug–Jul)	**(%E.V.)**		**(%E.V.)**		**(%E.V. > 5, p < 0.05)**
	T =365	T=183	30≥T>7	7≥T≥2	
1981–82	9.6	2.1	30.8	29.4	46 (5.2), 19 (5.8)
1982–83	3.4	6.5	39.7	29.9	24 (5.2)
1983–84	7.1	0.4	34.0	33.0	20 (5.0)
1984–85	12.8	0.2	25.5	34.9	61 (5.1), 52 (5.1)
1985–86	3.2	1.5	31.5	35.4	30 (7.2)
1986–87	10.4	0.2	28.9	50.0	—
1987–88	8.5	3.2	34.0	35.8	—
1988–89	11.6	1.8	34.9	38.7	—
1989–90	19.9	7.3	31.2	28.3	—
1990–91	8.9	1.2	36.9	32.7	16 (5.1)
1991–92	5.2	4.3	38.5	31.7	17 (5.0), 13 (5.5)
1992–93	4.3	3.8	27.4	33.0	73 (5.4), 61 (7.9), 30 (5.2)
1993–94	5.4	—	31.2	43.5	—
1994–95	13.5	3.7	33.5	33.3	91 (6.4), 24 (8.0)
1995–96	12.3	5.6	30.4	26.6	91 (8.6), 73 (10.5)
1996–97	10.0	1.2	31.8	33.2	121 (5.8)
1997–98	7.7	4.2	42.2	31.4	21 (7.9)

Table 3. Equations, correlation coefficients (*r*) and number of data points (n) used in AOU (μmol kg^{-1}), NC_T (μmol kg^{-1}), nutrient (μmol kg^{-1}) and Salinity–temperature (°C) regressions and their anomalies for the selected ENACW samples.

Regression equation	***r***	**n**
$S\ (\pm0.05) = 35.792(\pm0.003) + 0.121(\pm0.002) \times [\theta - 13]$	+0.94	395
$AOU(\pm8.8) = 21.9(\pm0.5) - 12.0\ (\pm0.4) \times [\theta - 13]$	–0.82	390
$NC_Tcor\ (\pm8.6) = 917(\pm1) - 19.5(\pm0.4) \times [\theta - 13]$	–0.92	382
$NO_3^-\ (\pm1.3) = 6.1(\pm0.1) - 3.43(\pm0.07) \times [\theta - 13]$	–0.94	382
$HPO_4^{2-}(\pm0.08) = 0.38(\pm0.01) - 0.180(\pm0.004) \times [\theta - 13]$	–0.92	375
$SiO_4H_4\ (\pm0.5) = 1.89(\pm0.04) - [1.04(\pm0.03) - 0.26(\pm0.02) \times (\theta - 13)] \times [\theta - 13]$	–0.94	379
$\Delta AOU(\pm4.8) = 6.8(\pm0.2) \times \Delta NO_3^-$	+0.84	359
$\Delta NC_Tcor(\pm6.9) = 6.5(\pm0.5) \times \Delta NO_3^-$	+0.57	359
$\Delta NO_3^-(\pm0.7) = 16.7(\pm0.6) \times \Delta HPO_4^{2-}$	+0.83	359
$\Delta NO_3^-(\pm0.8) = 2.4(\pm0.1) \times \Delta SiO_4H_4$	+0.79	359

Table 4. Average±SD photosynthetic parameters (P_m^B, α^B, E_k), depth of the photic layer ($\mathbf{Z_{0.1\%}}$, 0.1% of incident light at the surface), integrated primary production rate (**PP**) and integrated chlorophyll–a concentration (Chl–*a*), in the photic layer of **PCCC** and in the coastal waters during the GALICIA–XII (Sep 1991), MORENA–I (May 1993) and CD110b (Jan 1998) cruises. Data for Coastal (upwelled) and oceanic (stratified) waters, during the Bg9815c cruise (June–Jul 1998), are also presented for comparative purposes.

Cruise–Domain	P_m^B	α^B	$\mathbf{E_k}$	$\mathbf{Z_{0.1\%}}$	**PP**	**Chl–*a***
	$\frac{\mathrm{gC}}{\mathrm{gChl}\cdot\mathrm{h}}$	$\frac{\mathrm{gC(gChl)^{-1}h^{-1}}}{\mu\mathrm{molm^{-2}s^{-1}}}$	$\frac{\mu\mathrm{mol}}{\mathrm{m^2}\cdot\mathrm{s}}$	m	$\frac{\mathrm{mg\,C}}{\mathrm{m^2}\cdot\mathrm{d}}$	$\frac{\mathrm{mg\,Chl}}{\mathrm{m^2}}$
Sep. 1991–PCCC	4.14±2.77	0.027±0.015	216±199	81±14	356±134	28±6
Sep. 1991–Coastal	7.39±3.82	0.049±0.025	186±143	70±5	2126±709	32±5
May 1993–PCCC	4.77±2.1	0.063±0.03	103±77	97±26	776±295	36±7
May 1993–Coastal	4.08±2.7	0.052±0.03	120±108	71±1	393±108	30±11
Jan. 1998–PCCC	1.42±0.4	0.04±0.02	41±13	55±4	138±44	54±6
Jul. 1998–Coastal	2.93±0.8	0.02±0.004	156±70	70	2057	219
Jul. 1998–Ocean	4.15±1.65	0.039±0.014	126±67	80±15	506±116	24±5

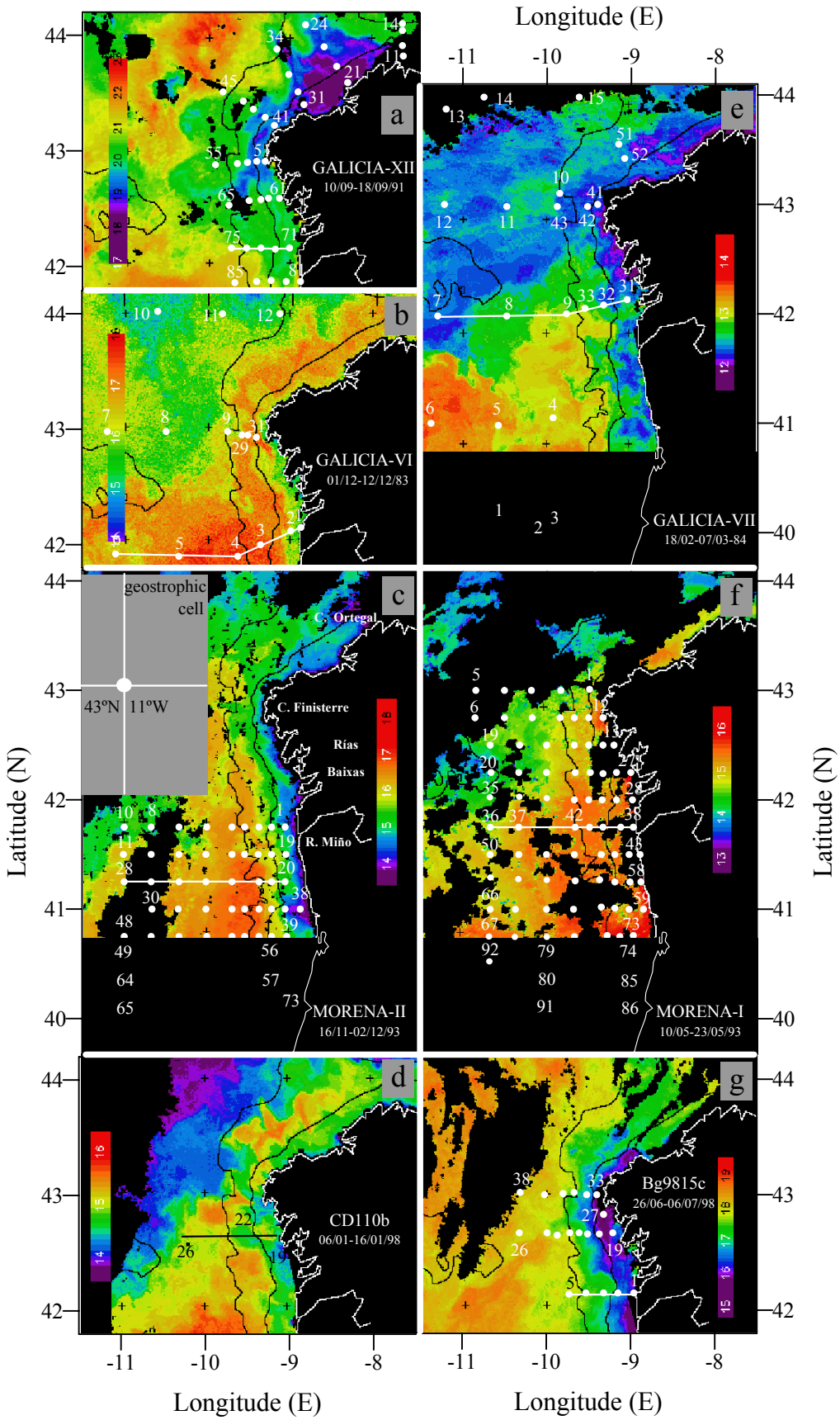

Álvarez-Salgado et al., Fig. 1

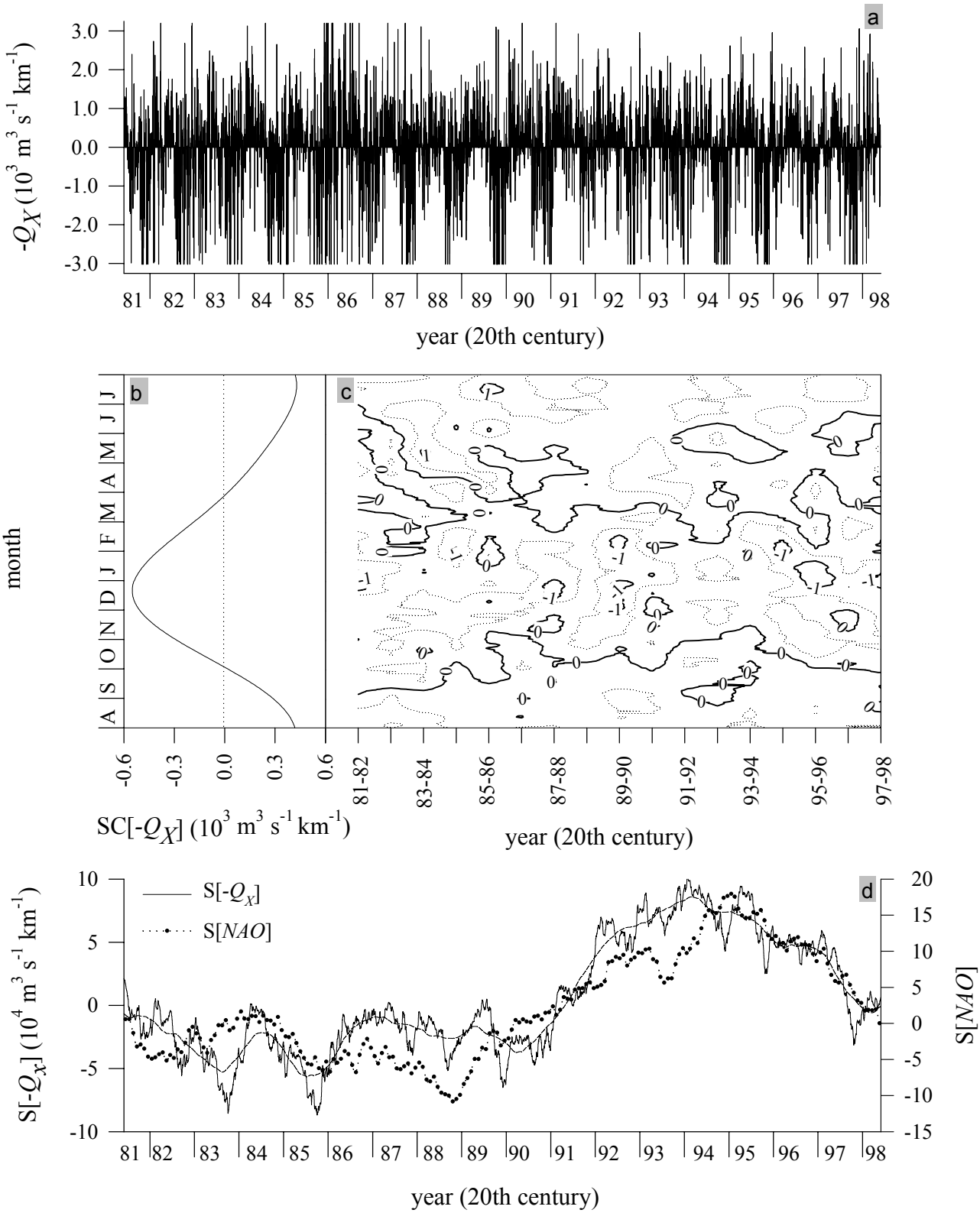

Alvarez-Salgado et al., Fig. 2

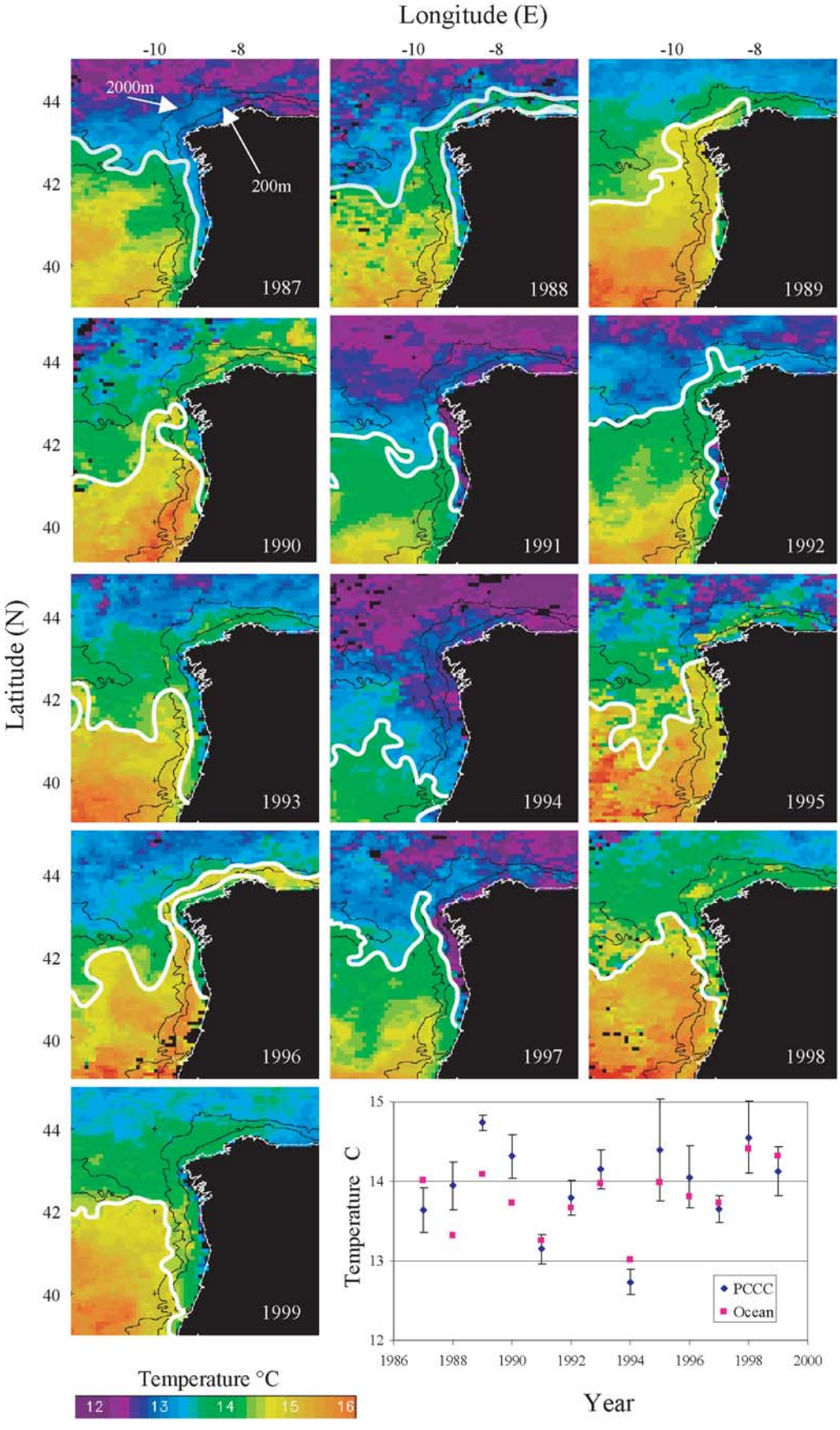

Álvarez-Salgado et al., Fig. 3

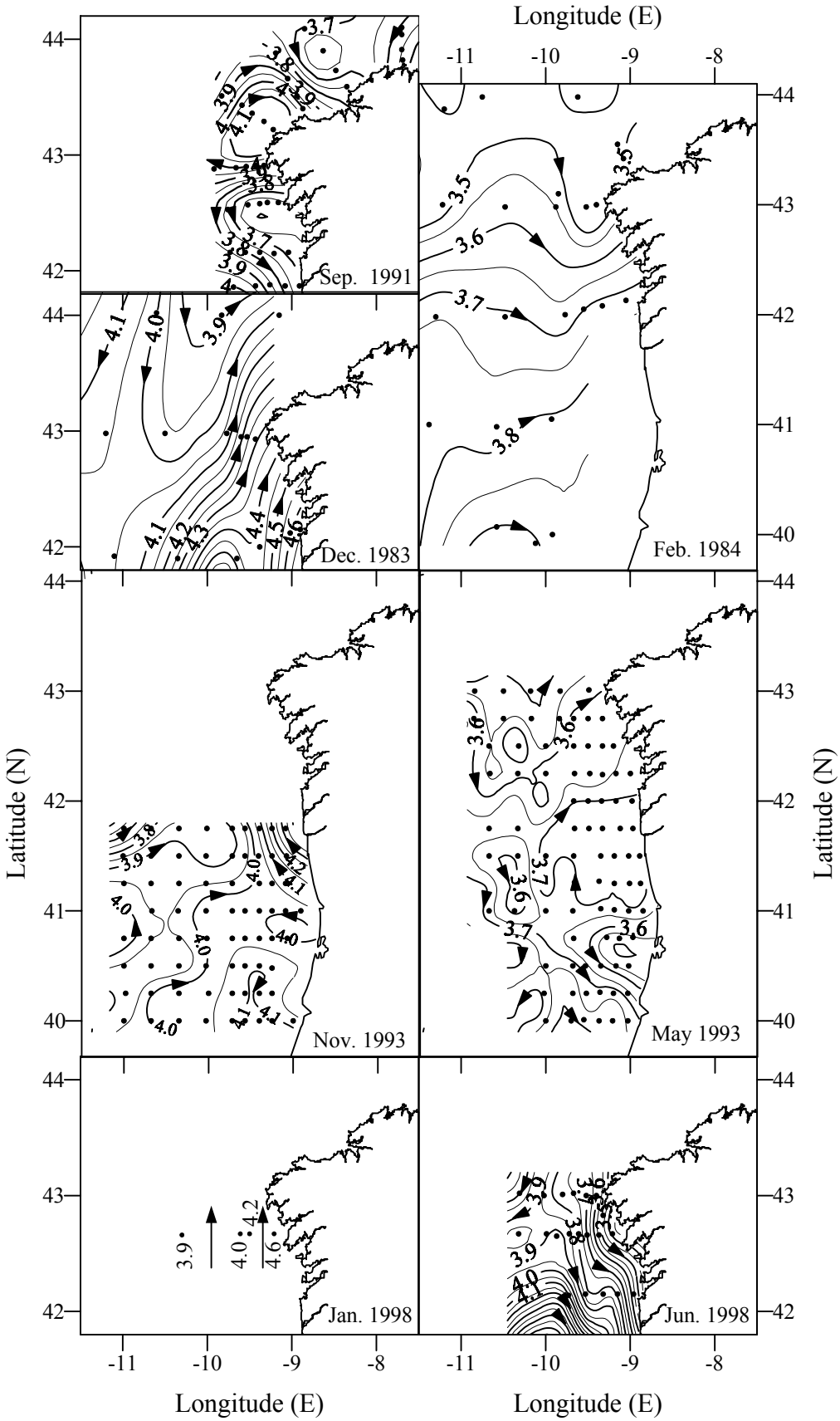

Alvarez-Salgado et al., Fig. 4

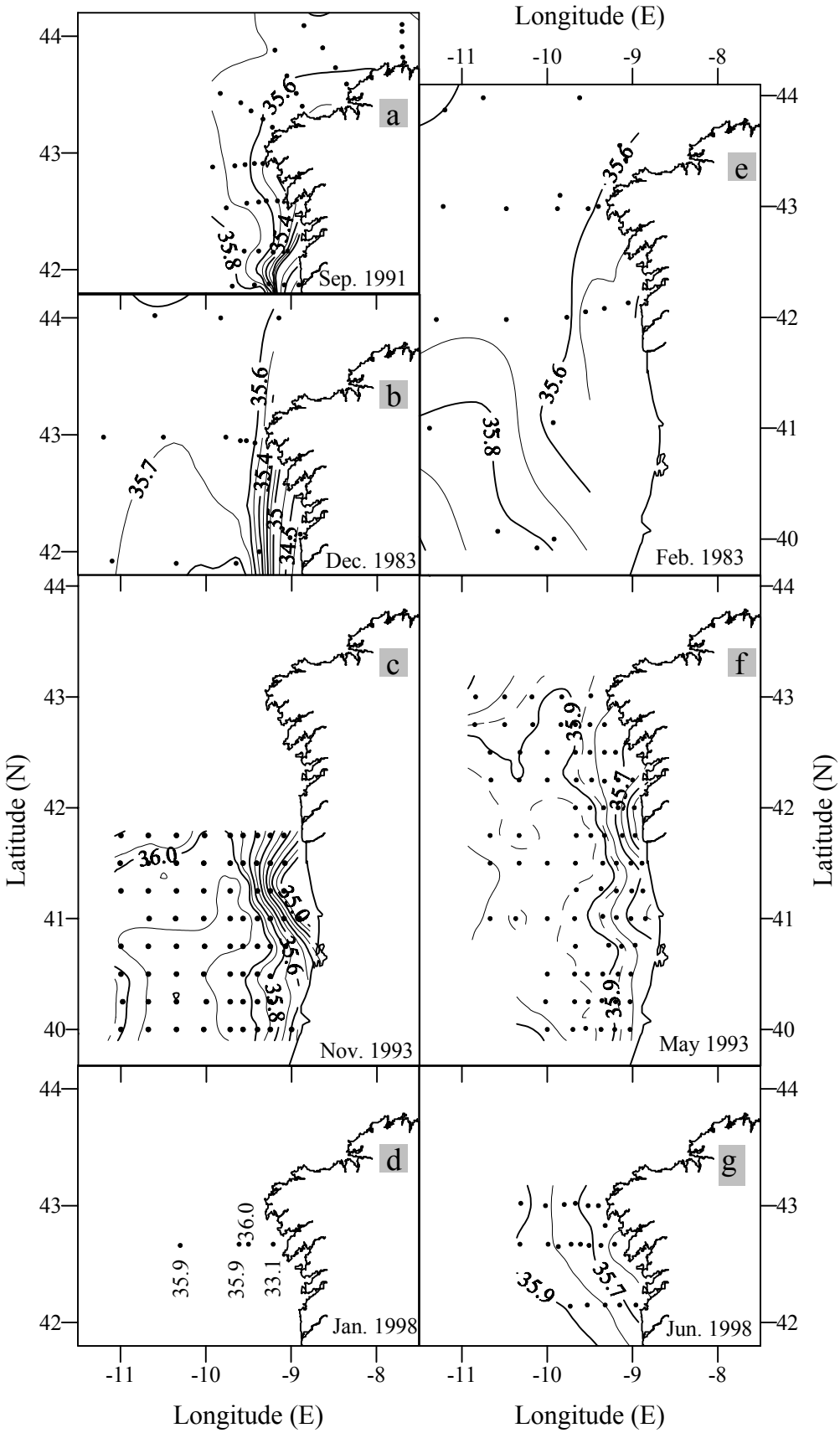

Alvarez-Salgado et al., Fig. 5

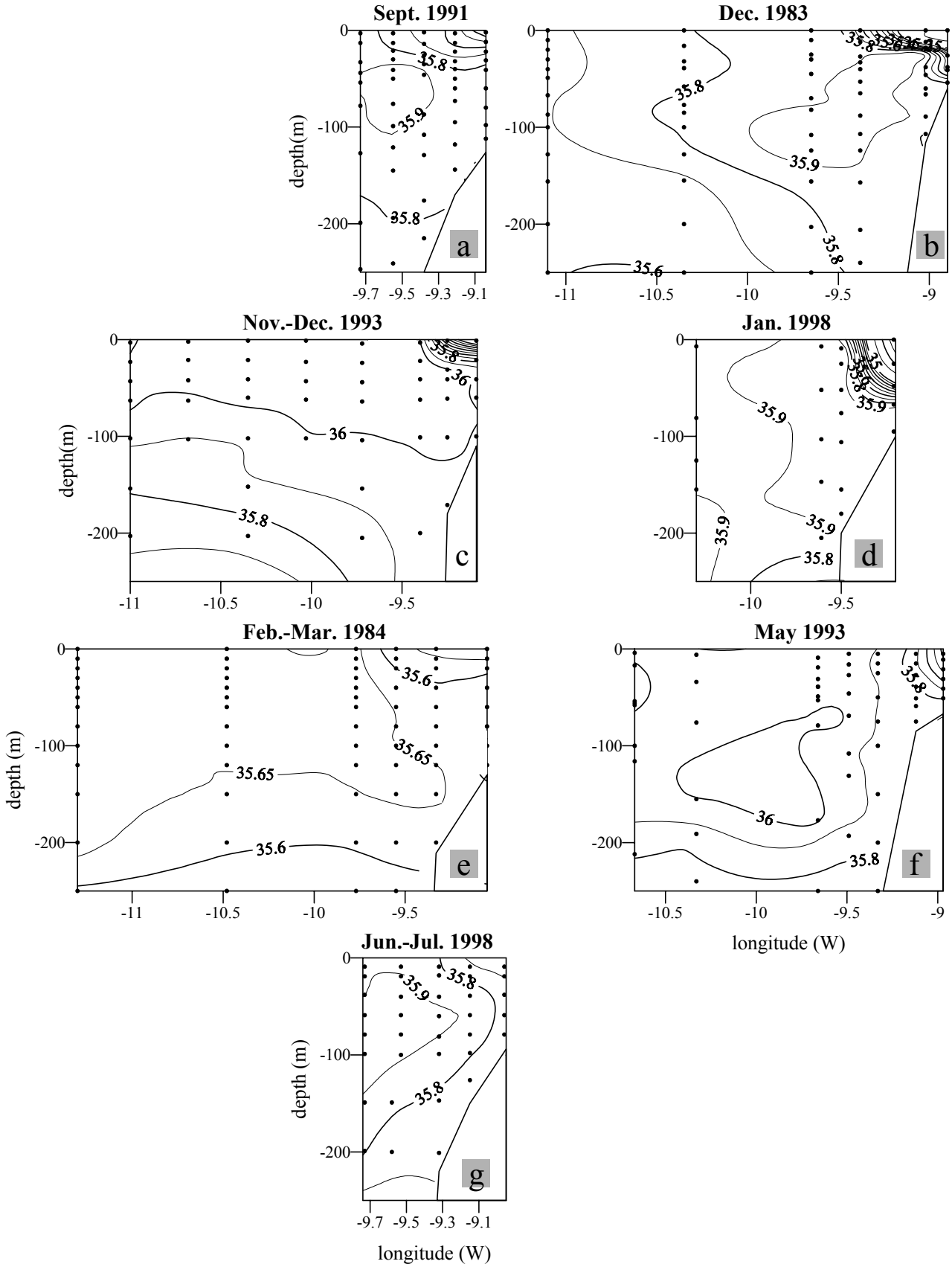

Alvarez-Salgado et al., Fig. 6

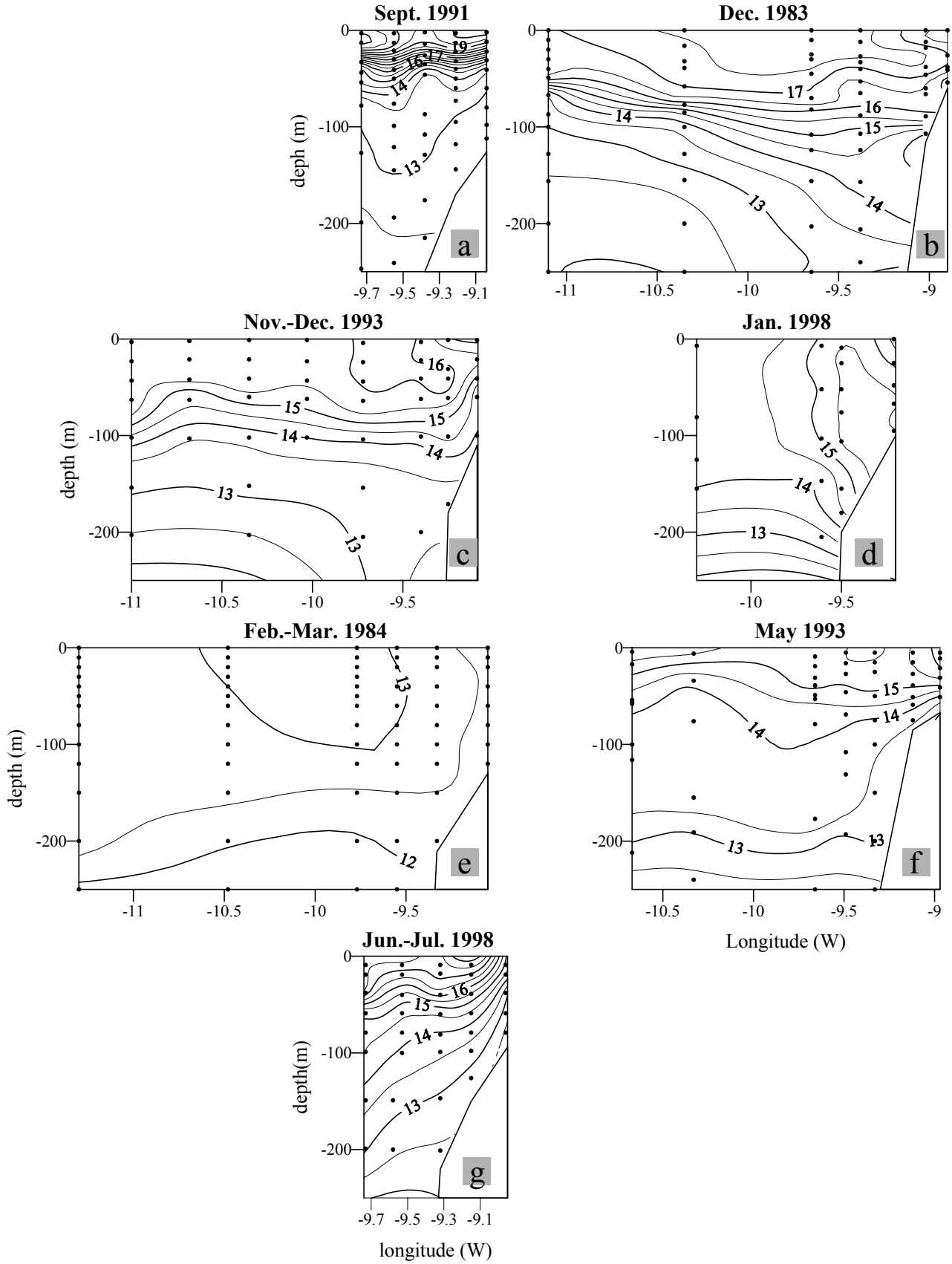

Alvarez-Salgado et al., Fig. 7

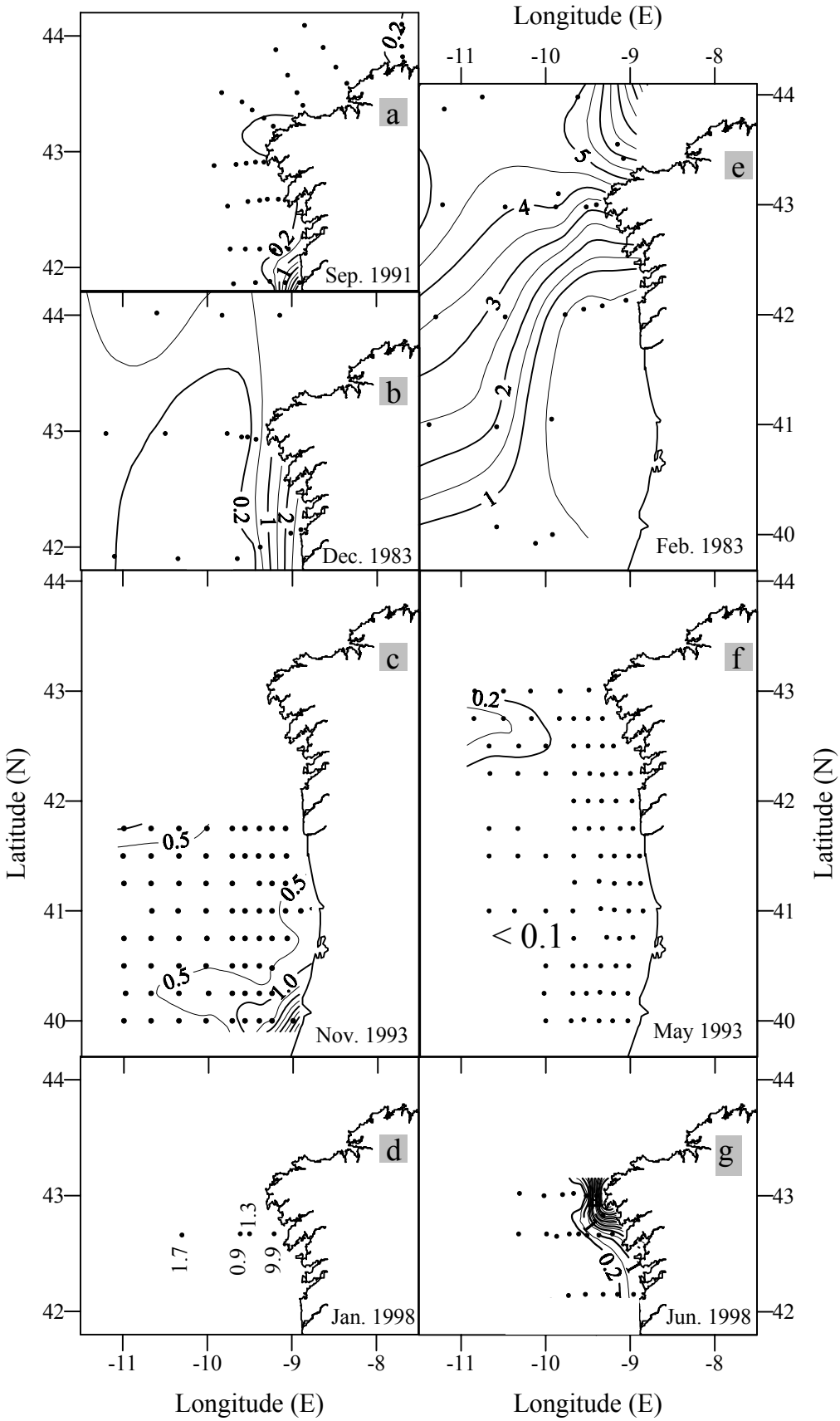

Alvarez-Salgado et al., Fig. 8

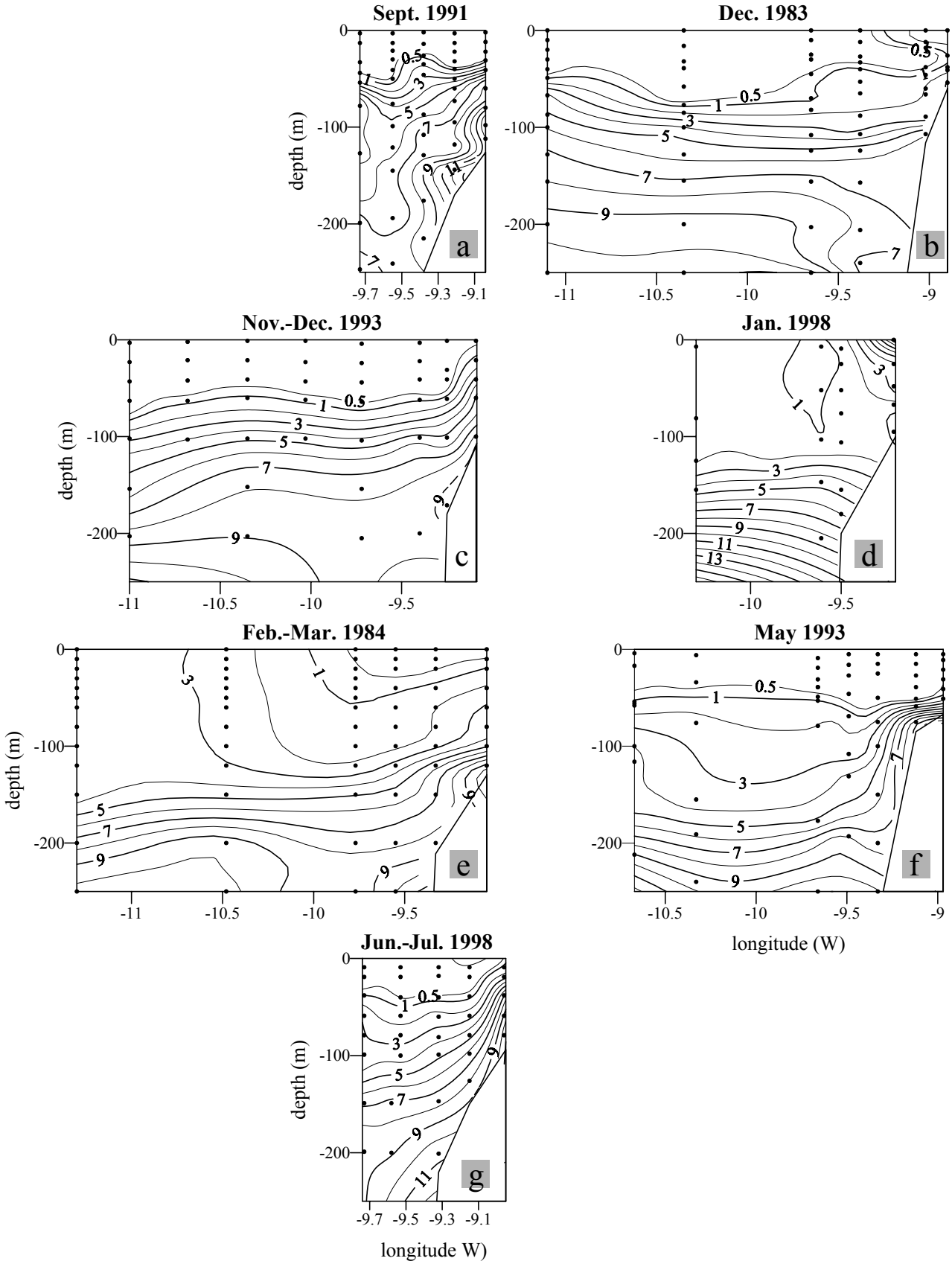

Alvarez-Salgado et al., Fig. 9

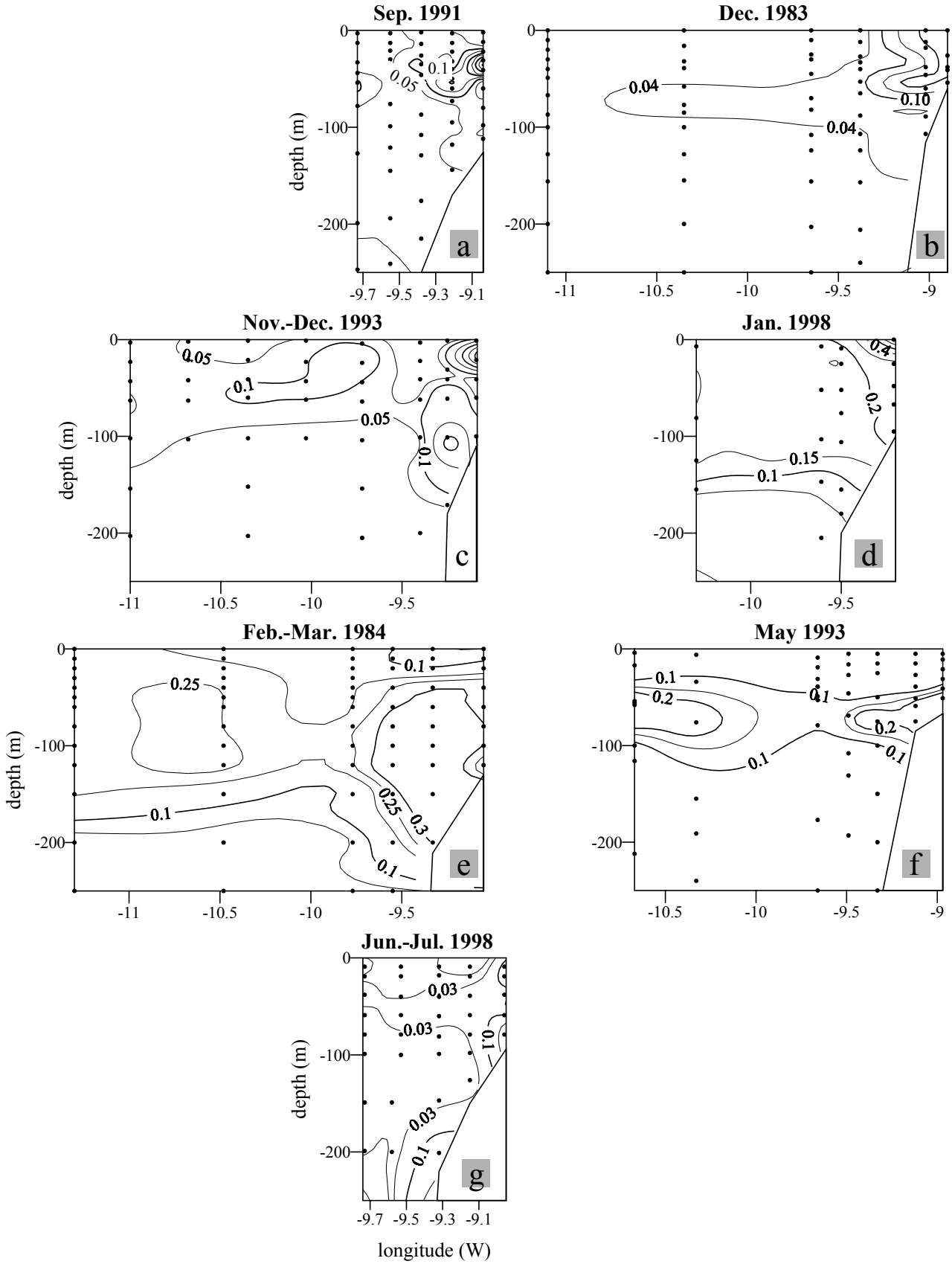

Alvarez-Salgado et al., Fig. 10

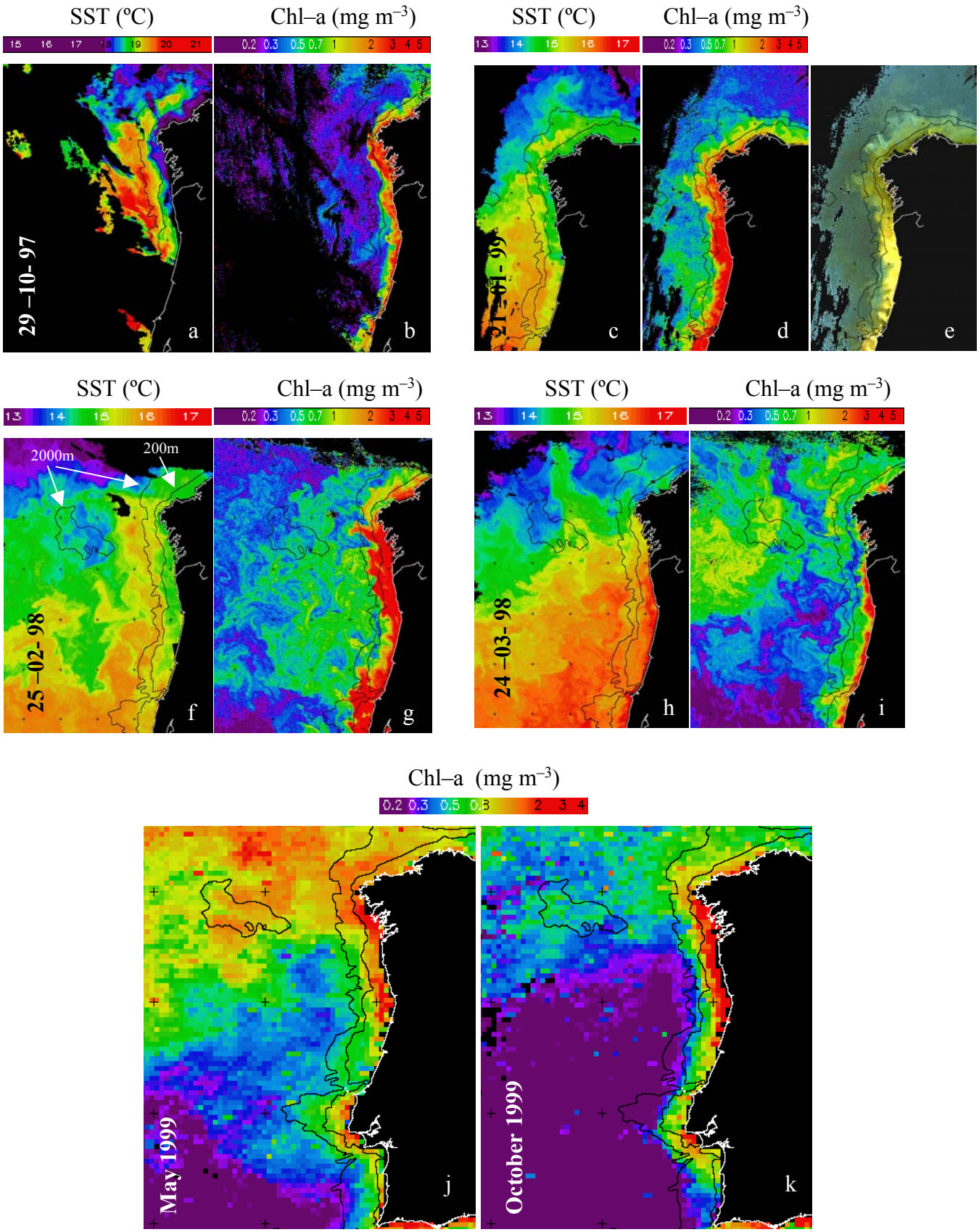

Alvarez-Salgado et al., Fig. 11

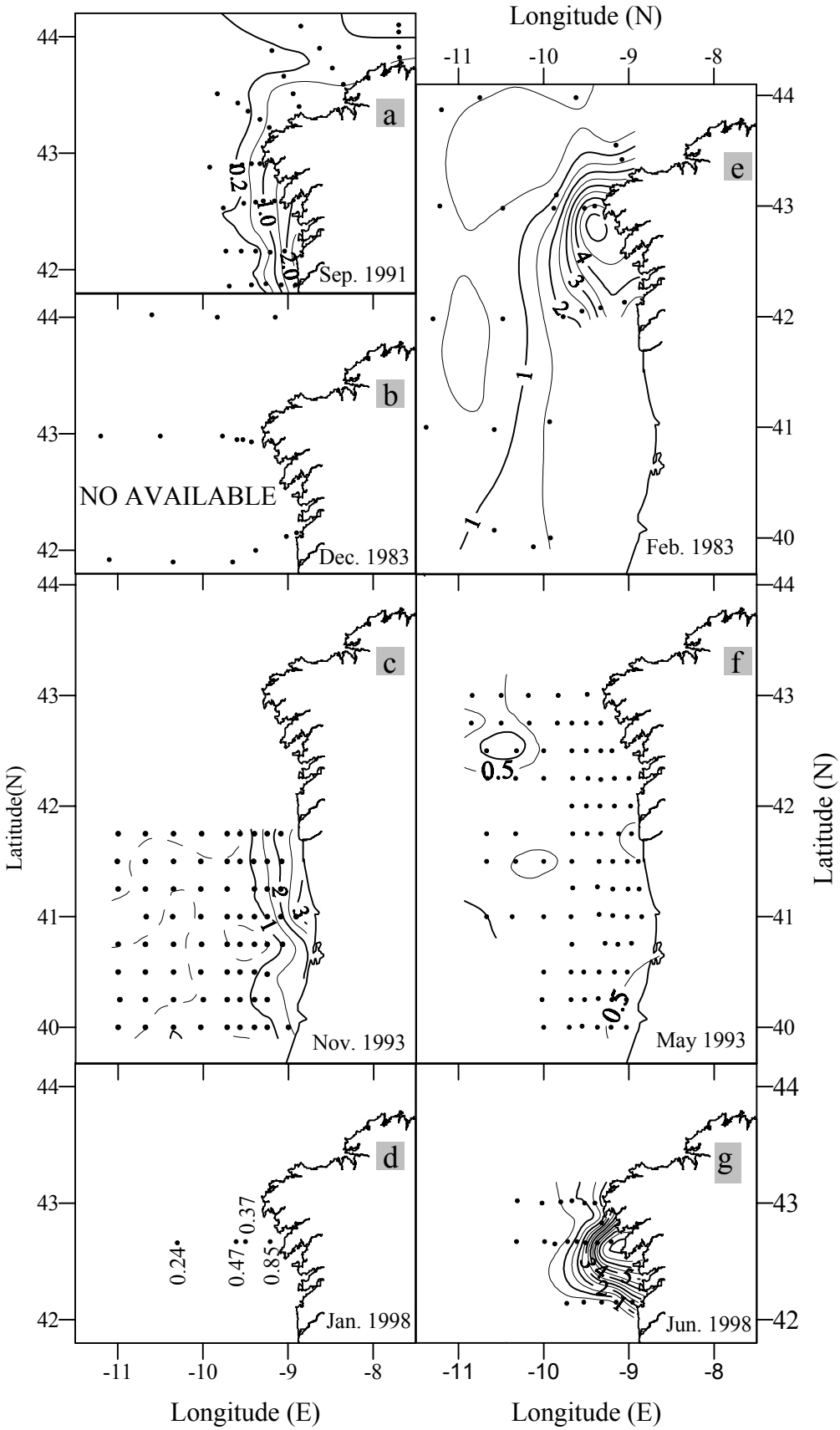

Alvarez-Salgado et al., Fig. 12

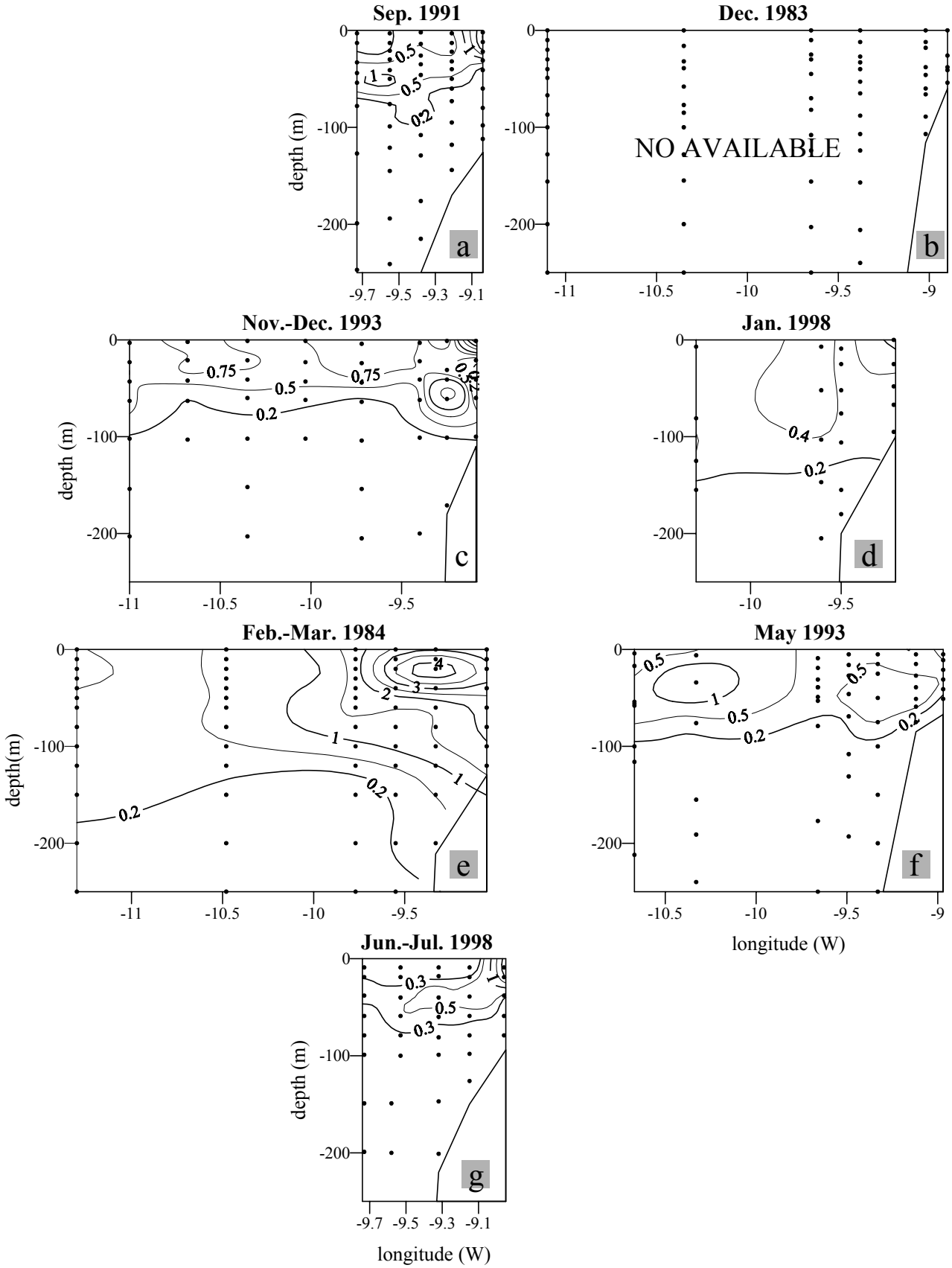

Alvarez-Salgado et al., Fig. 13

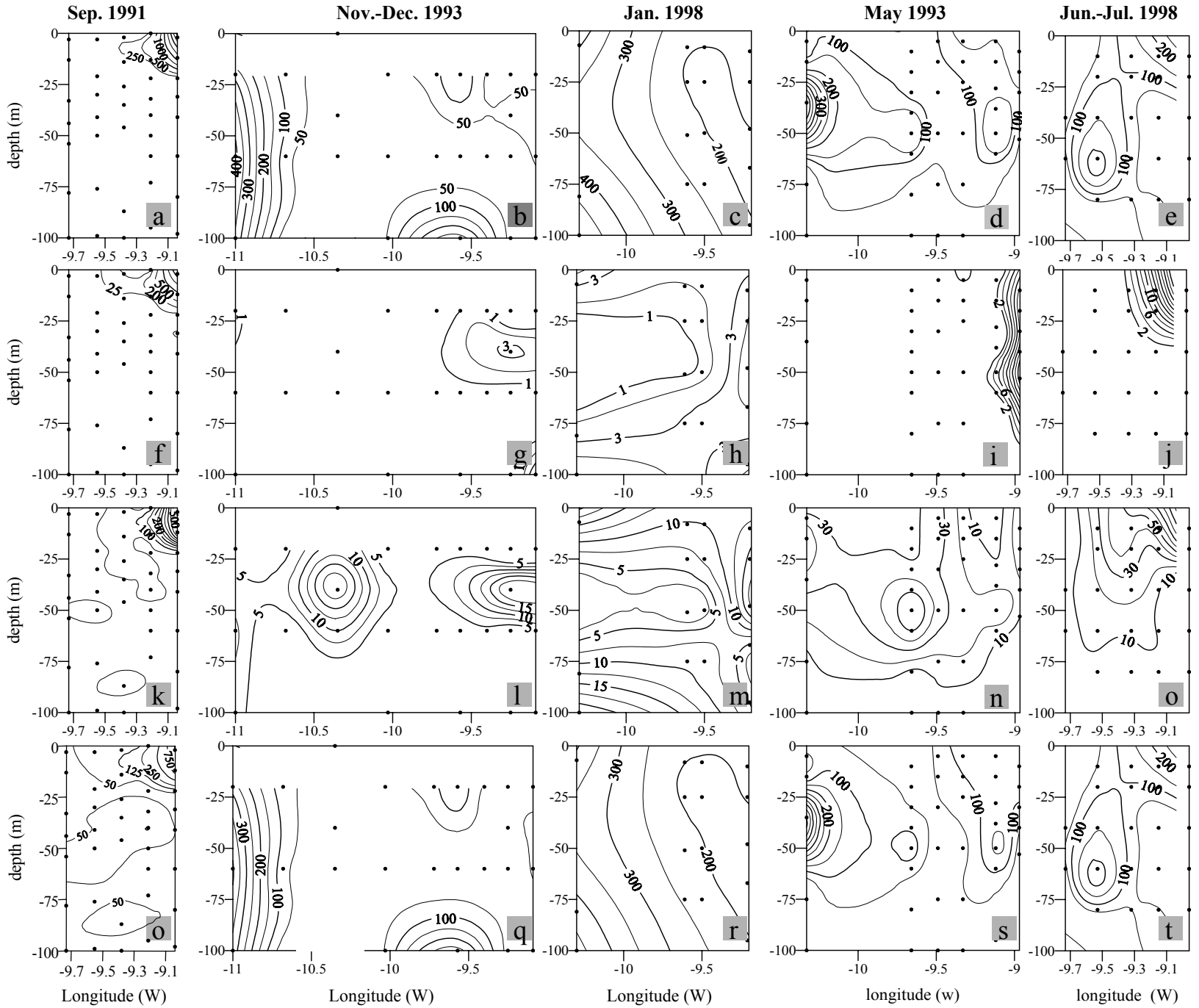

Álvarez-Salgado et al. Fig. 14